Molecular endpoints of Ca^{2+}/calmodulin- and voltage-dependent inactivation of $Ca_V1.3$ channels

Michael R. Tadross,[2] Manu Ben Johny,[2] and David T. Yue[1,2]

[1]Department of Neuroscience and [2]Department of Biomedical Engineering, The Johns Hopkins University School of Medicine, Baltimore, MD 21205

Ca^{2+}/calmodulin- and voltage-dependent inactivation (CDI and VDI) comprise vital prototypes of Ca^{2+} channel modulation, rich with biological consequences. Although the events initiating CDI and VDI are known, their downstream mechanisms have eluded consensus. Competing proposals include hinged-lid occlusion of channels, selectivity filter collapse, and allosteric inhibition of the activation gate. Here, novel theory predicts that perturbations of channel activation should alter inactivation in distinctive ways, depending on which hypothesis holds true. Thus, we systematically mutate the activation gate, formed by all S6 segments within $Ca_V1.3$. These channels feature robust baseline CDI, and the resulting mutant library exhibits significant diversity of activation, CDI, and VDI. For CDI, a clear and previously unreported pattern emerges: activation-enhancing mutations proportionately weaken inactivation. This outcome substantiates an allosteric CDI mechanism. For VDI, the data implicate a "hinged lid–shield" mechanism, similar to a hinged-lid process, with a previously unrecognized feature. Namely, we detect a "shield" in $Ca_V1.3$ channels that is specialized to repel lid closure. These findings reveal long-sought downstream mechanisms of inactivation and may furnish a framework for the understanding of Ca^{2+} channelopathies involving S6 mutations.

INTRODUCTION

Ca^{2+} entry through high voltage–gated Ca^{2+} (Ca_V1 and Ca_V2) channels selectively triggers numerous neurobiological processes, including transmitter release, gene transcription, and memory formation (Berridge et al., 2000). Fitting with these vital roles, $Ca_V1/2$ channels are highly regulated through a variety of feedback mechanisms that inactivate channels in response to either intracellular Ca^{2+} elevations (e.g., Ca^{2+}-dependent inactivation [CDI]) or voltage-dependent conformational changes (e.g., voltage-dependent inactivation [VDI]). The initial steps involved in these prototypic forms of regulation have been studied extensively. For example, it is known that Ca^{2+} binds to a constitutively associated calmodulin (CaM), which then interacts with other sites on the channel to induce CDI (Lee et al., 1999, 2003; Peterson et al., 1999; Zühlke et al., 1999; Erickson et al., 2001, 2003; Pitt et al., 2001; Mori et al., 2004; Dick et al., 2008; Tadross et al., 2008). Similarly, it is well accepted that voltage-dependent conformational changes of $Ca_V1/2$ channels are initially triggered by movement of four homologous voltage-sensing domains, each consisting of transmembrane helices S1–S4 (Swartz, 2008). These rearrangements open the intracellular gate, comprised of distal S6 segments (Liu et al., 1997; Xie et al., 2005), and predispose the channel to VDI. Although more is known about the initiation of these regulatory events, the transduction and ultimate endpoint mechanisms of these forms of Ca^{2+} channel modulation have eluded consensus. Given the physiological importance of VDI and CDI, and the likelihood that certain Ca^{2+} channelopathies involve defects in the end stage rather than initial steps of these regulatory processes (Kraus et al., 1998, 2000; Splawski et al., 2004, 2005; Hoda et al., 2005; Hohaus et al., 2005; Barrett and Tsien, 2008), these downstream mechanisms represent crucial unknowns in the field.

Currently, three main hypotheses exist regarding end-stage actions of inactivation across the family of voltage-gated channels, although none has been definitively established for Ca^{2+} channels. The first and most prominent idea (case 1) is that of a cytoplasmic inactivation particle that binds to cytoplasmic aspects of the permeation pathway when the channel is open, thereby plugging the pore (Fig. 1 C, case 1) (Armstrong and Bezanilla, 1977). In molecular terms, the inactivating particle was identified as an amino-terminal "ball and chain" for K^+ channels undergoing N-type inactivation (Hoshi et al., 1990), and as a "hinged loop" connecting homologous domains III and IV of voltage-gated Na^+ channels (West

Correspondence to David T. Yue: dyue@jhmi.edu; or Michael R. Tadross: mtadross@gmail.com

Abbreviations used in this paper: CaM, calmodulin; CDI, Ca^{2+}-dependent inactivation; GHK, Goldman-Hodgkin-Katz; VDI, voltage-dependent inactivation.

The Rockefeller University Press $30.00
J. Gen. Physiol. Vol. 135 No. 3 197–215
www.jgp.org/cgi/doi/10.1085/jgp.200910308

et al., 1992). For Ca^{2+} channels, this idea takes the form of a "hinged lid" comprised of the loop between homologous domains I and II. As evidence, Ca^{2+} channel VDI can be significantly altered by swapping the I-II loop between different $Ca_V1/2$ channels, by mutating the I-II loop, or by using different β subunits that bind to the I-II loop (Bourinet et al., 1999; Stotz et al., 2000, 2004; Bernatchez et al., 2001; Stotz and Zamponi, 2001; Dafi et al., 2004). Furthermore, mutating certain S6 regions (the putative I-II loop binding site) also disrupts VDI (Kraus et al., 1998, 2000; Stotz et al., 2000, 2004; Stotz and Zamponi, 2001; Splawski et al., 2004, 2005; Hoda et al., 2005; Hohaus et al., 2005; Raybaud et al., 2006, 2007; Barrett and Tsien, 2008). Finally, overexpressing a I-II loop peptide alone enhances VDI (Cens et al., 1999), suggesting that even the free peptide represents a lid that can directly bind and occlude the pore. The involvement of such a hinged-lid mechanism in CDI is less clear and based mainly on observations that certain molecular manipulations similarly alter VDI and CDI. These data have been used to argue that VDI and CDI share a common endpoint (Cens et al., 1999; Kim et al., 2004; Findeisen and Minor, 2009).

A second hypothesis proposes a collapse of the selectivity filter (Fig. 1 C, case 2), as in P-type inactivation of K^+ channels (also known as C-type inactivation) (Choi et al., 1991; Hoshi et al., 1991). The selectivity filter (P loops within S5–S6 linkers) resides near the extracellular surface of the membrane (Doyle et al., 1998), opposite the intracellular activation gate. Thus, P-type inactivation is sensitive to manipulations near the extracellular surface of the pore (López-Barneo et al., 1993; Yellen et al., 1994; Loots and Isacoff, 2000; Cordero-Morales et al., 2007). Likewise, some have suggested that this mechanism pertains to $Ca_V1/2$ channels (Zhang et al., 1994), partly because VDI is modulated by toxins and cations that bind to the extracellular face of the channel (Zhang et al., 1994; Jones et al., 1999; Beedle et al., 2002). For CDI, there are potential indications that CDI may be affected by mutating the selectivity filter or substituting the permeant ion (Zong et al., 1994; Babich et al., 2005, 2007), motivating the notion that CDI might be linked to selectivity filter rearrangements.

A third idea (Fig. 1 E, case 3) is that Ca^{2+} channel inactivation works by allosteric inhibition of the intracellular activation gate. Unlike the previous two hypotheses, where the pore of an inactivated channel is constitutively nonconductive, an allosterically inactivated channel would favor closure, yet still open intermittently. Evidence for this mechanism comes from single-channel Ca^{2+} records of $Ca_V1.2$, in which CDI reduces the frequency of opening without completely silencing channels (Imredy and Yue, 1994). During VDI, in contrast, single-channel Ba^{2+} records reveal the complete absence of openings (Imredy and Yue, 1994), suggesting that CDI and VDI use different endpoints. Further indications of the distinct nature of VDI and CDI come from two Ca_V mutations that alter VDI with little effect on CDI (Barrett and Tsien, 2008), and from the immobilization of gating charge by VDI, but not CDI (Hadley and Lederer, 1991; Shirokov et al., 1993; Jones et al., 1999; Barrett and Tsien, 2008).

To distinguish among these potential downstream effects of CDI, this paper develops theoretical analyses that make a discriminating prediction regarding Ca^{2+}/CaM-mediated Ca^{2+} channel regulation: mutations in the distal S6 transmembrane regions (the intracellular activation gate) should produce distinctive effects on activation and inactivation, depending on which mechanism holds true. To date, studies of select S6 mutations, mostly relating to heritable channelopathies, have in fact detected effects on VDI, CDI, and activation (Kraus et al., 1998, 2000; Stotz et al., 2000, 2004; Stotz and Zamponi, 2001; Splawski et al., 2004, 2005; Hoda et al., 2005; Hohaus et al., 2005; Raybaud et al., 2006, 2007; Barrett and Tsien, 2008). However, no systematic mutagenesis screen that would enable discrimination among hypotheses has previously been performed. Here, to fully exploit our theoretical distinctions, we undertake comprehensive scanning mutagenesis of the intracellular S6 segments of all four domains of $Ca_V1.3$. This channel isoform exhibits robust CaM-mediated CDI, making $Ca_V1.3$ a useful prototype for the $Ca_V1/2$ channel family (Yang et al., 2006; Dick et al., 2008; Tadross et al., 2008). The S6 mutations produce dramatic functional effects in favor of allosteric modulation of activation gating as the CDI endpoint.

For VDI, our S6 mutagenesis screen implicates an entirely different mechanism. The pattern of effects supports a hinged-lid scheme with an additional "shield" that repels lid closure. This shield represents an apt specialization enabling $Ca_V1.3$ channels to maintain opening despite sustained activation, such as in ribbon synapses. After "removal" of the shield via mutagenesis, we confirm hinged-lid receptor sites within S6 domains, homologous to those identified previously in $Ca_V1.2$ channels (Hohaus et al., 2005). Overall, these findings furnish key mechanistic advances and a rich backdrop for understanding heritable diseases that involve mutations in these S6 domains.

MATERIALS AND METHODS

Molecular biology

Point mutations of $Ca_V1.3$ (α_{1D}) were made in rat $\alpha_{1D,short}$ (Xu and Lipscombe, 2001). A 2.3-kb stretch containing IS6 and IIS6 (bounded by BsiWI and Eco47III) was cloned into Zero Blunt TOPO (Invitrogen), yielding NT_D-$TOPO_{I\text{-}II}$. Similarly, NT_D-$TOPO_{III\text{-}IV}$ contained IIIS6 and IVS6 (bounded by BglII and XbaI). QuikChange (Agilent Technologies) was used to mutate individual residues to proline within these TOPO clones, and the relevant region was then transferred into α_{1D} by digest and ligation. All segments subject to PCR were verified by sequencing.

Transfection of HEK293 cells

For electrophysiology, HEK293 cells were cultured on 10-cm plates and transiently transfected by a calcium phosphate protocol (Peterson et al., 1999). We combined 8 µg each of cDNAs encoding channel α_1 subunit, rat brain $\alpha_{2\delta}$ (Tomlinson et al., 1993), and rat brain β_{2a} (Perez-Reyes et al., 1992) or β_{1b} (Pragnell et al., 1991), along with 2 µg SV40 T antigen. All subunits were driven by a cytomegalovirus promoter. Experiments were done 1–2 d later.

Whole cell electrophysiology

Whole cell recordings were obtained at room temperature (Axopatch 200A; Axon Instruments). Electrodes were pulled from borosilicate glass capillaries (MTW 150-F4; World Precision Instruments), with 1–3-MΩ resistances, before 80% series resistance compensation. Currents were filtered at 2 kHz (four-pole Bessel), and P/8 leak subtraction was used. The internal solution contained (in mM): 124 $CsMeSO_3$, 5 $CsCl_2$, 1 $MgCl_2$, 4 MgATP, 10 HEPES, pH 7.4, and 5 EGTA at 295 mOsm adjusted with $CsMeSO_3$. External solutions contained (in mM): 130 TEA-$MeSO_3$, 10 HEPES, pH 7.4, and 10 $CaCl_2$ or $BaCl_2$ at 300 mOsm adjusted with TEA-$MeSO_3$.

Analysis methodology

VDI and *CDI* (Fig. 2 A) were calculated as follows: $VDI(t) = 1 - I_{Ba}(t)/I_{Ba}(t_{peak,Ba})$ and $CDI(t) = 1 - (I_{Ca}(t)/I_{Ca}(t_{peak,Ca}))/(I_{Ba}(t)/I_{Ba}(t_{peak,Ba}))$, where $I_{Ca}(t)$ and $I_{Ba}(t)$ are whole cell currents in Ca^{2+} and Ba^{2+}, respectively, and $t_{peak,Ca}$ and $t_{peak,Ba}$ correspond to the time of peak current after depolarization. This method of calculating *CDI* accounts for baseline *VDI* with a ratiometric correction as described in several recent reports (Barrett and Tsien, 2008; Tadross et al., 2008; Findeisen and Minor, 2009). Due to the rapid onset of CDI in $Ca_V1.3$, $t_{peak,Ca}$ often apparently occurred earlier than $t_{peak,Ba}$. To minimize the extent to which this could degrade our estimates of *CDI*, we limited $t_{peak,Ba}$ (and $t_{peak,Ca}$) to the first 50 ms of depolarization. Thus, certain constructs have a negative metric of VDI_{300}, which indicates very slowly activating channels. We chose the VDI_{300} metric for brevity of representation, so as to allow a single metric to represent both the strong VDI of "shield-disrupting" mutants (i.e., those in the right half of Fig. 5 C) and the comparative lack of VDI in other constructs (i.e., those in the left third of Fig. 5 C). Spot checks of VDI_{1000} measurements showed good agreement with the rank order of VDI indicated by VDI_{300}. For $I_{PEAK}(V)$ relations (e.g., Fig. 2 C), we did not constrain the time of peak current, and thus these curves accurately reflect steady-state channel activation. The $I_{PEAK}(V)$ curves reflect the product of two terms, as given by $I_{PEAK}(V) = P_{O\text{-}PEAK}(V) \cdot i_N(V)$, where $P_{O\text{-}PEAK}(V)$ is the relative open probability shown in Fig. 2 D, and $i_N(V)$ is a normalized unitary current relation (Fig. 2 C, dashed curve) closely approximating the scaled Goldman-Hodgkin-Katz (GHK) relation below.

$$i_N(V) = -g \cdot (V - V_S) \cdot \frac{1}{\exp[(V - V_S) \cdot z_{GHK} F/(RT)] - 1} + i_{LEAK}(V)$$

Because S6 mutations leave unchanged the conductance of an open channel (Tadross et al., 2008), we maintain a constant shape of $i_N(V)$, and thus fix $(z_{GHK} F/RT)^{-1} = +12$ mV, and $V_S = +20$ mV for all constructs. The scale factor *g*, representing a composite of single-channel conductance and channel number, is freely adjusted in each construct for proper normalization. For subtle nonlinearities in leak at large *V*, we included a small leak correction term, $i_{LEAK}(V)$, which amounts to the difference between dashed and solid curves at very positive *V* (e.g., Fig. 2 C).

Homology modeling of the $Ca_V1.3$ S5-S6 domains

For the closed-state molecular model of the $Ca_V1.3$ S5-S6 segments, the KcsA (Protein Data Bank accession no. 1BL8) crystal structure was used as template (Doyle et al., 1998). Modeller 9v4 (Eswar et al., 2006) was used to generate 50 models, from which the structure with the lowest objective function was chosen. Modeller builds three-dimensional atomic structures by optimizing an objective function based on CHARMM energy terms and a set of distance and dihedral angle restraints from the alignment of target and template sequences. The four domains of $Ca_V1.3$ were arranged in a clockwise configuration as viewed from the extracellular surface by analogy to the orientation of voltage-gated sodium channels (Li et al., 2001). An analogous procedure was used for the open conformation, with the KvAP crystal structure as template (Protein Data Bank accession no. 1ORQ) (Jiang et al., 2003).

Online supplemental material

Fig. S1 is an extended version of Fig. 3 that includes all constructs from our mutagenesis screen. This allows for comprehensive visual comparison of trends across all S6 residues of the four homologous domains comprising $Ca_V1.3$ channels. Fig. S1 is available at http://www.jgp.org/cgi/content/full/jgp.200910308/DC1.

RESULTS

Theory of S6: mutation effects on activation and inactivation

To provide a structural framework for considering the effects of S6 mutations, we constructed a homology model of the S5 and S6 transmembrane segments of $Ca_V1.3$, based on the KcsA and KvAP crystal structures for the closed and open conformations, respectively (Doyle et al., 1998; Jiang et al., 2003). We favored the K_VAP over $K_V1.2$ structure because both $Ca_V1.3$ and K_VAP lack the S6 domain "PVP" kink present in $K_V1.2$. The P loops, which connect S5 and S6, were excluded because of poor conservation between K^+ and Ca^{2+} channels. Fig. 1 A shows the CLUSTAL sequence alignments used for modeling. The top rows show K^+ channel alignments, and the rows below display Ca^{2+} channel alignments for all four domains. In addition to $Ca_V1.3$, two related Ca^{2+} channels ($Ca_V1.2$ and $Ca_V2.1$) are aligned to facilitate comparison with previous work. For ease of reference, we have assigned a common set of "S6 coordinates," as denoted by the numbered scale at the bottom of Fig. 1 A. Fig. 1 B displays the resulting closed and open $Ca_V1.3$ homology models, which resemble prior models of $Ca_V1.2$ (Huber et al., 2000; Zhorov et al., 2001; Lipkind and Fozzard, 2003; Raybaud et al., 2006, 2007; Beyl et al., 2007). In the closed state, the S6 helices point inward to form a central "bundle crossing" that, by homology to K^+ channels, acts as a closed intracellular gate impermeant to the passage of ions. In the open conformation, the S6 helices splay outward, consistent with free passage of permeant ions. This structural model of the intracellular gate agrees well with functional cysteine accessibility studies, which have been performed on the S6 segment of K_V1 (Liu et al., 1997) and the II-S6 segment of $Ca_V2.1$

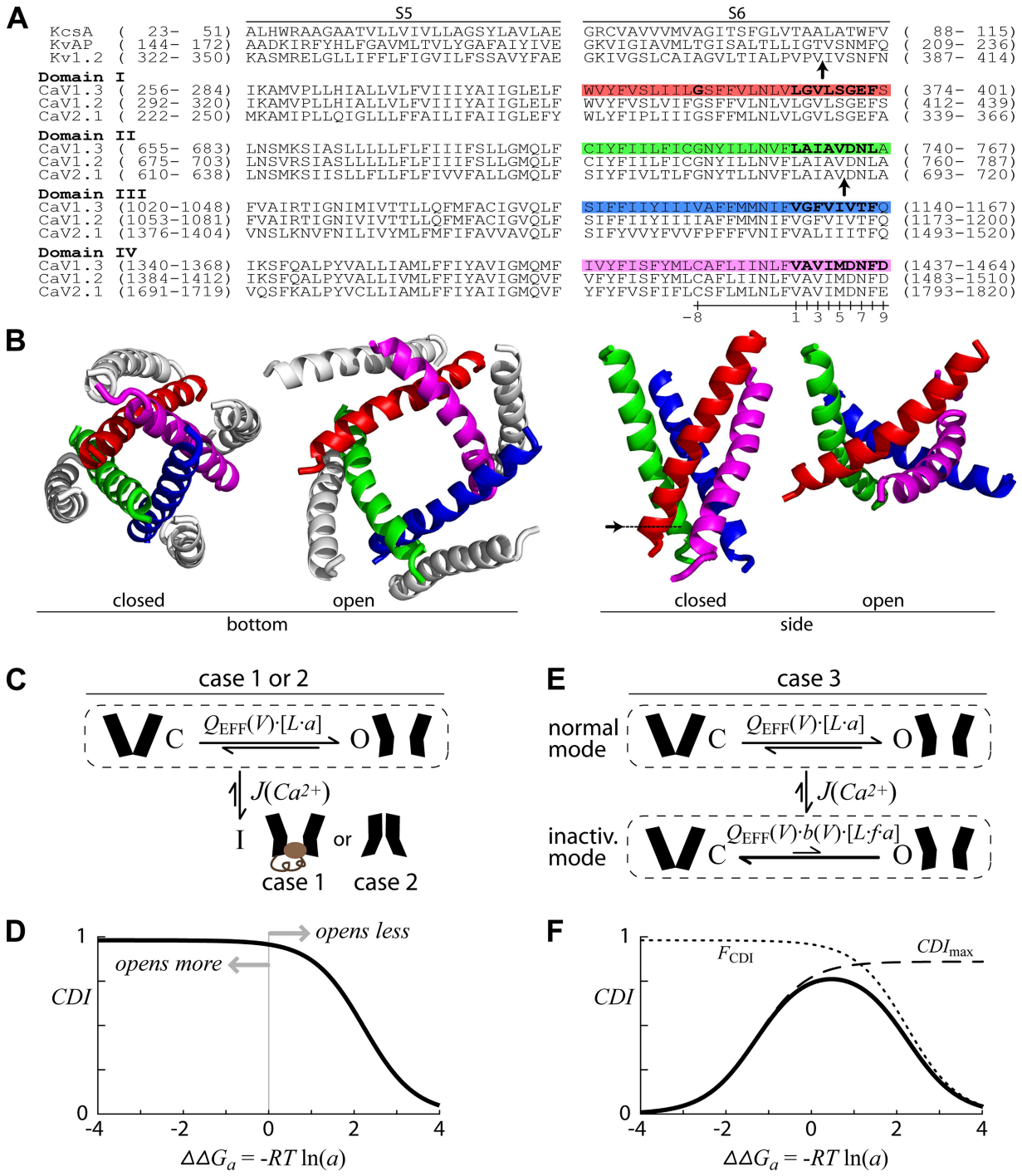

Figure 1. Structural and functional models of S6 domains. (A) CLUSTAL alignment of S5–S6 domains of three K^+ channels with known crystal structures (top) and the four domains of $Ca_V1.3$, $Ca_V1.2$, and $Ca_V2.1$. Arrows indicate putative location of the intracellular S6 gate, as determined from previous cysteine accessibility studies. $Ca_V1.3$ residues in bold indicate sites that were mutated to proline in this study. Colored highlights correspond to the color scheme used in B. Numbered scale defines a common set of "S6 coordinates" for ease of reference. (B) Structural homology model of $Ca_V1.3$ S5/S6 segments, based on KcsA (closed) and KvAP (open). Bottom and side views are shown. Arrow in the closed side view corresponds to the gate identified in A. (C and D) Theory of S6 mutation effects on a hinged-lid or selectivity filter collapse mechanism. In C, channels activate via a C↔O transition governed by voltage-sensing term $Q_{EFF}(V)$ and concerted gate-opening term L. Partitioning between normal and inactivated modes is driven by Ca^{2+} influx through the channel and is governed by $J(Ca^{2+}) \approx P_{O\text{-}PEAK}/K_{eff}$. Note that these equilibrium coefficients represent the ratio of forward and reverse kinetic rate constants, which are not individually defined. (D) The predicted outcome if S6 mutations selectively perturb L by the factor a. Eq. 4 was used with parameters: $Q_{EFF}(V) \cdot L = 0.8$; $1/K_{eff} = 50$. $R \cdot T = 0.6$ kCal/mole throughout. (E and F) Theory of S6 mutation effects on an allosteric CDI mechanism. Channels occupy either a normal (top row of E) or inactivated gating mode (bottom row). In both modes, channels activate via a C↔O scheme as defined in C; however, channels in the inactivated mode open less often because $f < 1$.

TABLE I

Summary of symbols

Symbol	Definition
$Q_{EFF}(V)$	Effective equilibrium constant corresponding to movement of the S1–S4 voltage sensors (Fig. 1, C and E)
L	Equilibrium constant representing the subsequent ("late") concerted opening of the S6 intracellular gate (Fig. 1, C and E)
a	S6 mutations act by multiplying L by this scaling factor
$\Delta G_{CO,WT}$	Energy required to activate the native (wild-type) channel (Eq. 1)
$\Delta\Delta G_a$	Additional energy needed to activate a mutant versus native channel (Eq. 1)
$\Delta V_{1/2}$	Change in voltage required for half-maximal opening of mutant versus native channels
$J(Ca^{2+})$	Effective equilibrium constant describing the Ca^{2+}-mediated transition between active (top row) and inactive (bottom row) conformations in Fig. 1 (C and E); $J(Ca^{2+}) \approx P_{O\text{-}PEAK}/K_{eff}$
K_{eff}	A constant closely analogous to the effective Ca^{2+} dissociation constant for CDI, which has been experimentally estimated at a value far less than unity (Tadross et al., 2008)
$P_{O\text{-}PEAK}$	Peak open probability shortly after membrane depolarization (Eq. 2)
$P_{O\text{-}SS}$	Steady-state open probability after a prolonged depolarization; for cases 1 and 2, $P_{O\text{-}SS} = P_{O\text{-}PEAK} \cdot (1 - F_{CDI})$ (Eq. 3); for case 3, $P_{O\text{-}SS} = P_{O\text{-}PEAK} \cdot (1 - F_{CDI} \cdot CDI_{max})$ (Eq. 5)
CDI	CDI, defined as fraction of peak current lost at steady state; for cases 1 and 2, $CDI = F_{CDI}$ (Eq. 4); for case 3, $CDI = F_{CDI} \cdot CDI_{max}$ (Eq. 5)
F_{CDI}	Fraction of inactivated channels at steady state (Eq. 4)
CDI_{max}	Fractional change in open probability of the normal mode versus the inactivated mode (Eq. 5)
VDI_{50}, VDI_{300}	Experimental measure of VDI after 50 and 300 ms of depolarization (see Fig. 2 A and Materials and methods)
CDI_{50}, CDI_{300}	Experimental measure of CDI after 50 and 300 ms of depolarization (see Fig. 2 A and Materials and methods)

(Xie et al., 2005). The arrows in Fig. 1 A indicate the critical gate location: residues to the right of the arrows (i.e., intracellular to the gate) are always accessible to intracellular agents, but residues to the left are accessible only in the open- (not closed-) channel conformation (Liu et al., 1997; Xie et al., 2005). The arrow in Fig. 1 B marks the homologous intracellular gate location in $Ca_V1.3$.

These homology models (Fig. 1 B) help visualize ways in which S6 domains could play a role in channel inactivation. First, because the S6 segments line the cytoplasmic aspect of the channel pore, certain residues are well positioned to serve as a binding site for a cytoplasmic inactivation particle (case 1), particularly in the open conformation. Alternately, in response to channel opening, the S6 segments could transmit mechanical forces to the P loop region and thus induce inactivation by selectivity filter collapse akin to that in K^+ channels (case 2). Finally, inactivation could involve an allosteric modulation of the very same intracellular gate involved in activation, which is comprised of the S6 segments (case 3).

Given this perspective, we considered how S6 mutagenesis can distinguish among these proposals. The key is this: although the proposed mechanisms differ considerably, all three share a common voltage-dependent activation process that then couples to inactivation in distinctive ways. Thus, S6 mutations that perturb this common pathway turn out to impact inactivation differentially, depending on which end-stage mechanism holds true. These discriminating predictions apply most directly to the CDI process, as follows.

To capture the essence of voltage activation, we represent this process in the compact form shown in the top row of Fig. 1 (C and E), wherein the equilibrium constant between closed (C) and open (O) states is given by the product of two terms: a voltage-dependent term $Q_{EFF}(V)$, corresponding to movement of the S1–S4 voltage sensors, and a voltage-independent term L, representing the subsequent ("late") concerted opening of the S6 intracellular gate (Zagotta et al., 1994). For convenience, the variables defined here and below are summarized in Table I. Despite its apparent simplicity, this formulation is rather general and can precisely represent the steady-state opening of multistate activation schemes with numerous closed states if $Q_{EFF}(V)$ becomes a complex function of voltage, as described in our companion paper (see Tadross and Yue in this issue). Of greater relevance to our immediate concerns, we note that S6 mutations should directly alter the concerted opening step (L) because of the fundamental involvement of S6 segments in this final gating transition (compare closed and open conformations in Fig. 1 B). Mutations of this type would act by multiplying L by a scaling factor a (Fig. 1, C and E), and the parameter $Q_{EFF}(V)$ would remain unchanged if S6 mutations have no collateral effects on the voltage-sensing domains. Finally, in terms of energetics, the overall free energy required

Partitioning between normal and inactivated modes is driven by Ca^{2+} influx through the channel as in C. (E) The predicted outcome if S6 mutations selectively perturb L by the factor a. CDI (solid curve) is the product of two terms: F_{CDI} (dotted line) and CDI_{max} (dashed line). Eq. 5 was used with parameters: $Q_{EFF}(V) \cdot L = 0.8$, $1/K_{eff} = 50$, and $f \cdot b(V) = 0.14$.

per mole of transitions from a closed (C) to open (O) conformation, ΔG_{CO}, would be:

$$\Delta G_{CO} = -R\cdot T\cdot \ln(Q_{EFF}(V)\cdot L\cdot a) = \underbrace{-R\cdot T\cdot \ln(Q_{EFF}(V)) - R\cdot T\cdot \ln(L)}_{\Delta G_{CO,WT}} \underbrace{-R\cdot T\cdot \ln(a)}_{\Delta\Delta G_a}, \quad (1)$$

where R is the universal gas constant, T is temperature, and V is transmembrane voltage. $\Delta G_{CO,WT}$ is the energy required to activate the native (wild-type) channel. Part of this energy is electrical ($-R\cdot T\cdot \ln(Q_{EFF}(V))$), and the remainder is chemical ($-R\cdot T\cdot \ln(L)$). For mutant channels, $\Delta\Delta G_a$ represents the additional chemical energy needed to activate a mutant versus native channel. Because channel activation is known to be kinetically faster than inactivation, we can calculate peak open probability shortly after membrane depolarization, assuming occupancy of only the two states in the top row (Fig. 1 ,C and E):

$$P_{O\text{-}PEAK} = \frac{Q_{EFF}(V)\cdot L\cdot a}{1 + Q_{EFF}(V)\cdot L\cdot a} \quad (2)$$

With this activation framework, we next considered the effects on inactivation for cases 1 and 2. Both cases are represented by the same state diagram in Fig. 1 C because they both feature a nonconductive inactivated conformation. Because CDI is driven by elevations of intracellular Ca^{2+} very near channels, the ratio of inactivated to noninactivated channels must be a function of this Ca^{2+}, which we term $J(Ca^{2+})$. Despite the apparent simplicity of Fig. 1 C, which depicts the inactivation process as a single transition governed by $J(Ca^{2+})$, this formalism is rather general. In particular, the behavior of the scheme in Fig. 1 C is shown to correspond well to the detailed CDI scheme in our companion paper (Tadross and Yue, 2010), which allows for inactivation from both closed and open states, and dissects the CDI process into separate events representing Ca^{2+} binding to CaM, CaM/channel binding, and the final transduction of CDI. Thus, $J(Ca^{2+})$ in Fig. 1 C is a shorthand for transitions between numerous intermediate states. Given the "slow CaM" mechanism that predominates in $Ca_V1.3$ channels and our use of elevated intracellular Ca^{2+} buffering, $J(Ca^{2+})$ becomes a simple function of the time-averaged Ca^{2+} concentration (Tadross et al., 2008), which is proportional to $P_{O\text{-}PEAK}$ in Eq. 2. Specifically, $J(Ca^{2+}) \approx P_{O\text{-}PEAK}/K_{eff}$, where K_{eff} has been experimentally estimated at a value far less than unity (Tadross et al., 2008). Beyond Ca^{2+} binding to CaM, $J(Ca^{2+})$ could incorporate either the affinity of an inactivation particle for its pore-blocking binding site (case 1), or the efficacy with which mechanical forces transduce selectivity filter collapse (case 2). Importantly, the dependence of $J(Ca^{2+})$ on $P_{O\text{-}PEAK}$ arises because only open channels conduct the Ca^{2+} entry required for Ca^{2+} binding to CaM; this dependence is not necessarily due to any preferential state dependence of CDI transduction per se. Thus, the CaM/channel binding and ultimate CDI transduction events implicit within Fig. 1 C can occur from both open and closed conformations, as is shown explicitly in our companion paper (Tadross and Yue, 2010). Factoring in inactivation, the steady-state open probability after a prolonged depolarization becomes:

$$P_{O\text{-}SS} = P_{O\text{-}PEAK}\cdot(1 - F_{CDI}), \quad (3)$$

where F_{CDI} is the fraction of inactivated channels at steady state. Accordingly, for inactivation defined as the fraction of peak current lost at steady state, we have for cases 1 and 2:

$$CDI_{(case\,1\,or\,2)} = \frac{P_{O\text{-}PEAK} - P_{O\text{-}SS}}{P_{O\text{-}PEAK}} = F_{CDI} = \frac{J(Ca^{2+})}{1 + J(Ca^{2+})} = \frac{P_{O\text{-}PEAK}/K_{eff}}{1 + P_{O\text{-}PEAK}/K_{eff}} = \frac{P_{O\text{-}PEAK}}{K_{eff} + P_{O\text{-}PEAK}} = \frac{1}{1+K_{eff}}\cdot\frac{Q_{EFF}(V)\cdot L\cdot a}{K_{eff}/(1+K_{eff}) + Q_{EFF}(V)\cdot L\cdot a} \quad (4)$$

Notably, $F_{CDI} = J(Ca^{2+})/(1 + J(Ca^{2+}))$ by the definitions of an equilibrium constant and of F_{CDI} itself. If experiments are performed at a fixed voltage (e.g., at $V = 0$), Eq. 4 directly relates *CDI* to changes in the chemical energy of activation induced by mutation (parameter *a*). A plot of Eq. 4 (Fig. 1 D) makes a first experimentally important prediction: for cases 1 and 2, inactivation would decrease for mutations that reduce channel opening ($\Delta\Delta G_a > 0$).

This prediction could help distinguish in favor of case 1 or 2 and merits two comments. First, the predicted outcome in Fig. 1 D presumes that S6 mutations would have no major collateral effects on the inactivation machinery or the voltage-sensing domains. This is plausible for CDI, but less so for VDI, where S6 elements have been proposed as the very receptor for a hinged lid (Hohaus et al., 2005). Hence, the type of prediction here, and for the allosteric case 3 (below), pertains to CDI and would not be readily adapted to a VDI scenario. Other aspects of the S6 mutagenesis screen, described later, will point to VDI endpoint mechanisms. Second, for simplicity, Eq. 4 presumes that S6 mutations would only affect $J(Ca^{2+})$ via changes in $P_{O\text{-}PEAK}$. However, as shown in our companion paper (Tadross and Yue, 2010), this might not be the case if CDI were to proceed more readily from closed versus open states. Analysis in our companion work explicitly excludes this possibility and substantiates the prediction for cases 1 and 2 in Fig. 1 D that CDI will be maintained for mutations that favor channel opening (negative $\Delta\Delta G_a$) and diminished for those that hinder opening (positive $\Delta\Delta G_a$).

What if inactivation represents the allosteric modulation of opening (case 3)? In this scenario, channels can adopt one of two gating modes. In the "normal" mode (Fig. 1 E, top row), channels gate according to a

C↔O model identical to the activation process of the previous analyses. Unlike the prior mechanisms, channels in the "inactivated" mode (bottom row) are not completely silent; rather, they open less frequently because of an allosteric increase in the chemical energy needed for opening ($0 < f < 1$ in Fig. 1 E, inactivated mode). Also, because of constraints from thermodynamic cycles, the voltage-dependent term in the inactivated mode may become $Q_{EFF}(V) \cdot b(V)$, where the voltage-dependent function $b(V)$ can deviate from unity in the most general configurations. For the scheme in Fig. 1 E, the expression for inactivation (fraction of peak current lost at steady state) becomes:

$$CDI_{(case3)} = \frac{P_{O\text{-}PEAK} - P_{O\text{-}SS}}{P_{O\text{-}PEAK}} = F_{CDI} \cdot CDI_{max} \quad (5)$$

$$\text{where } CDI_{max} = \frac{P_{O\text{-}PEAK} - P_{O\text{-}INACTIVATED}}{P_{O\text{-}PEAK}} = \frac{(1 - f \cdot b(V))}{1 + Q_{EFF}(V) \cdot b(V) \cdot L \cdot f \cdot a}$$

Thus, for the allosteric scheme (case 3), CDI is the product of two terms. First, F_{CDI} is the fraction of channels in the inactivated mode at steady state, as specified in Eq. 4. Second, CDI_{max} is the fractional change in open probability of the normal mode ($P_{O\text{-}PEAK}$ in Eq. 2) versus the inactivated mode ($P_{O\text{-}INACTIVATED} = Q_{EFF} \cdot b(V) \cdot L \cdot a \cdot f/(1 + Q_{EFF} \cdot b(V) \cdot L \cdot a \cdot f)$). Thus, CDI_{max} is the apparent CDI (fraction of peak current lost at steady state) if all channels were to transition from the normal to the inactivated gating mode. Notably, $CDI_{max} < 1$ because inactivated channels open sparsely (i.e., $f > 0$). A plot of Eq. 5 (Fig. 1 F), obtained with the step voltage held at a constant V throughout, makes a key prediction for the allosteric mechanism: CDI should have a bell-shaped dependence on $\Delta\Delta G_a$, as follows. First, as for cases 1 and 2, mutations that diminish opening ($\Delta\Delta G_a > 0$) cause a reduction in F_{CDI} owing to the lack of Ca^{2+} entry needed to drive transition into the inactivated mode (Fig. 1 F, dotted curve). Second, mutations that promote opening ($\Delta\Delta G_a < 0$) diminish CDI_{max} (Fig. 1 F, dashed curve) because mutations that enhance opening in the normal gating mode also enhance opening within the inactivated mode. Notably, this trend is opposite to that for cases 1 and 2 (compare with Fig. 1 D). Accordingly, the full extent of CDI is now shown by the solid bell-shaped curve in Fig. 1 F.

Characterization of inactivation and activation of $Ca_V1.3$ channels

These predictions motivated systematic mutagenesis of the intracellular S6 gate of $Ca_V1.3$. As reference, Fig. 2 summarizes the behavior of wild-type $Ca_V1.3$. On channel activation by a depolarizing voltage step to 0 mV (Fig. 2 A), the modest decay of Ba^{2+} current (blue trace) reflects VDI observed in isolation. The additional rapid decay with Ca^{2+} as charge carrier (red trace) reflects the robust CDI of $Ca_V1.3$. Accordingly, these forms of inactivation can be quantified as shown in Fig. 2 A (scale bars to the right), which defines the metrics *VDI* and *CDI*. Note that the calculation of *CDI* accounts for baseline *VDI* with a ratiometric correction (Barrett and Tsien, 2008; Tadross et al., 2008; Findeisen and Minor, 2009), such that *CDI* represents the purely Ca^{2+}-dependent component of inactivation (see Materials and methods). Fig. 2 B displays these metrics at 50 and 300 ms of depolarization, as averaged over multiple cells.

Beyond inactivation, testing the predictions in Fig. 1 required assessment of $\Delta\Delta G_a$, the change in chemical energy required to activate mutant versus native channels. Toward this end, we determined the voltage dependence of channel open probability in native channels, based on measurements of peak Ba^{2+} currents (I_{PEAK}). As inactivation is very slow with this charge carrier, peak Ba^{2+} currents are a faithful reporter of peak open probability owing to the activation process. Accordingly, these currents were normalized (Fig. 2 C, data points) and fit by a smooth curve (Fig. 2 C, solid curve), which was specified by the product of a GHK unitary–current relation (Fig. 2 C, dashed curve) and a single Boltzmann activation relation (Fig. 2 D, solid curve). As elaborated in Materials and methods, the same GHK relation (but for amplitude scaling) was used to fit all constructs. Dividing the I_{PEAK} data points by this GHK relation yielded the desired activation curve for native channels, $P_{O/WT}(V)$ (Fig. 2 D, data points).

We next devised a technique to obtain the value of $\Delta\Delta G_a$ ($= -R \cdot T \cdot \ln(a)$) for mutant channels, which incorporates all information from the activation curves of various constructs. This technique not only presumes that S6 mutations leave $Q_{EFF}(V)$ unchanged, but also tests whether this presumption is well founded. Once this condition is satisfied, the analysis furnishes the value of $\Delta\Delta G_a$, regardless of the functional form of $Q_{EFF}(V)$. The method makes use of our prior framework, wherein wild-type channels have a $P_{O/WT}$ relation given by Eq. 2 with $a = 1$ (by definition), and mutant channels have a $P_{O/MUT}$ relation of the same form, with all parameters identical except for a. If we then solve for $P_{O/MUT}$ in terms of $P_{O/WT}$, the unknown terms in Eq. 2 ($Q_{EFF}(V)$ and L) cancel out, leaving a useful interrelation:

$$P_{O/MUT}(V) = \frac{a \cdot P_{O/WT}(V)}{(a-1) \cdot P_{O/WT}(V) + 1} \quad (6)$$

In practice, this relation enabled robust determination of parameter a. For example, a plot of the activation relation for S6 mutant L0759P, expressed as a function of its wild-type counterpart, is well fit by Eq. 6 with $a = 14$ (Fig. 2 E, solid black curve). This saturating relationship indicates that the L0759P mutant enhances activation (i.e., $a > 1$). Alternatively, mutations that diminish activation (i.e., $a < 1$) would yield an upwardly curved relation, as is the case for F1463P (dashed

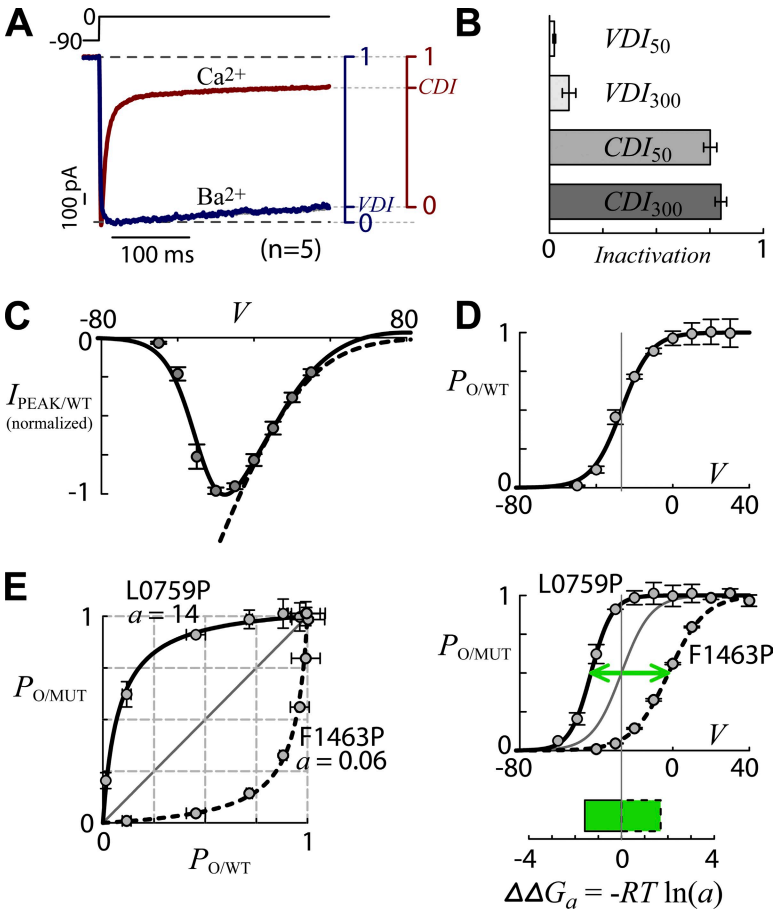

Figure 2. Baseline $Ca_V1.3$ behavior and method of calculating $\Delta\Delta G_a$. (A) Whole cell Ba^{2+} (blue) and Ca^{2+} (red) currents of $Ca_V1.3$ coexpressed with $\alpha_2\delta$ and β_{2a}, evoked by depolarization to 0 mV. Voltage pulse protocol (in mV) indicated above data trace here and throughout. Current scale bar is for Ca^{2+}; Ba^{2+} is scaled down approximately two to three times to match. Scales to the right define *VDI* and *CDI* metrics. See Materials and methods for details. (B) *VDI* and *CDI* (as defined in A) calculated after 50 and 300 ms of depolarization and averaged over many cells. Cell number (n) in A. Error bars are SEM. (C) Normalized $I_{PEAK}(V)$ relationship (see Materials and methods for details). Voltage (V) is in units of mV. Dashed relationship is proportional to the unitary current (before additional nonlinear leak correction). Cell number (n) in A. Error bars are SEM. (D) $P_{O\text{-}PEAK}(V)$, calculated by taking the ratio of data points from C and the leak-corrected unitary current relation. This yields the relative open probability (normalized to maximum P_O). Error bars are SEM from C divided by the unitary current relation. (E) Method for determining $\Delta\Delta G_a$. Graph on the left illustrates the determination of parameter a via Eq. 6. Top right graph follows the format of D, where V is in units of mV. $\Delta\Delta G_a$ (bottom right graph) is in units of kCal/mole. See Results for details.

curve). For both mutants, fits of Eq. 6 were highly constrained, yielding reliable estimates of $\Delta\Delta G_a = -R{\cdot}T{\cdot}\ln(a)$. Importantly, the close correspondence between data and theory (Fig. 2 E, left) supports the underlying presumption that S6 mutations do not alter $Q_{EFF}(V)$.

For added verification, we considered the outcome if a first-order Boltzmann approximation is assumed for the form of $Q_{EFF}(V)$, such that $Q_{EFF}(V) \approx \exp[(z \cdot F \cdot V)/(R \cdot T)]$. In this case, it can be shown that $\Delta\Delta G_a \approx z{\cdot}F{\cdot}\Delta V_{1/2}$, where $\Delta V_{1/2}$ is the change in voltage required for half-maximal opening of mutant versus native channels, z is the effective valence of the voltage-sensing modules, and F is Faraday's constant. For our exemplar mutants, $\Delta V_{1/2}$ (Fig. 2 E, right, green arrows) corresponds well to $\Delta\Delta G_a$ obtained from fits to Eq. 6 (green bars plotted below). Overall, there was a nearly linear relationship between $\Delta\Delta G_a$ and $\Delta V_{1/2}$, enabling us to estimate $z \approx 3.6$. However, we favor calculating $\Delta\Delta G_a$ via Eq. 6 (Fig. 2 E, left), as this method uses all of the data, makes no assumption on the form of $Q_{EFF}(V)$, and enables verification of the invariance of $Q_{EFF}(V)$ to the effects of S6 mutation.

S6 mutations alter activation, CDI, and VDI

Given this framework, we characterized the effects of S6 point mutations over all four domains of $Ca_V1.3$. Single proline substitutions were systematically introduced into regions spanning the S6 intracellular gate (Fig. 1 A, bold residues), thereby producing defined kinks in the straight helical elements portrayed in Fig. 1 B. The results are shown in Fig. 3, where each of four panels (A–D) pertains to a different domain, and each subpanel relates to a given construct according to the format in Fig. 2. For clarity, Fig. 3 displays only a subset of our mutagenesis screen. The complete set of S6 mutations is numerically summarized in Table II and graphically displayed in Fig. S1. Remarkably, every mutant produced readily measurable current, as illustrated by exemplar Ba^{2+} and Ca^{2+} traces at the far left of each subpanel (blue and red, respectively). Exemplar wild-type currents are overlaid for comparison (gray). For the population data shown in the middle of each subpanel, vertical lines mark the wild-type profiles for VDI, CDI, half-activation voltage, and $\Delta\Delta G_a$. Deviations from these are indicated as colored horizontal arrows. In this manner, we could readily appreciate a multitude of dramatic effects, distributed over all four domains. First, strong changes in activation were produced, with maximal deviations of $\Delta V_{1/2}$ approximating ±40 mV, corresponding to $\Delta\Delta G_a$ values of ±3 kcal/mole (e.g., Fig. 3, A and B, G0394P and I0761P, respectively). Interestingly, the direction of the effect

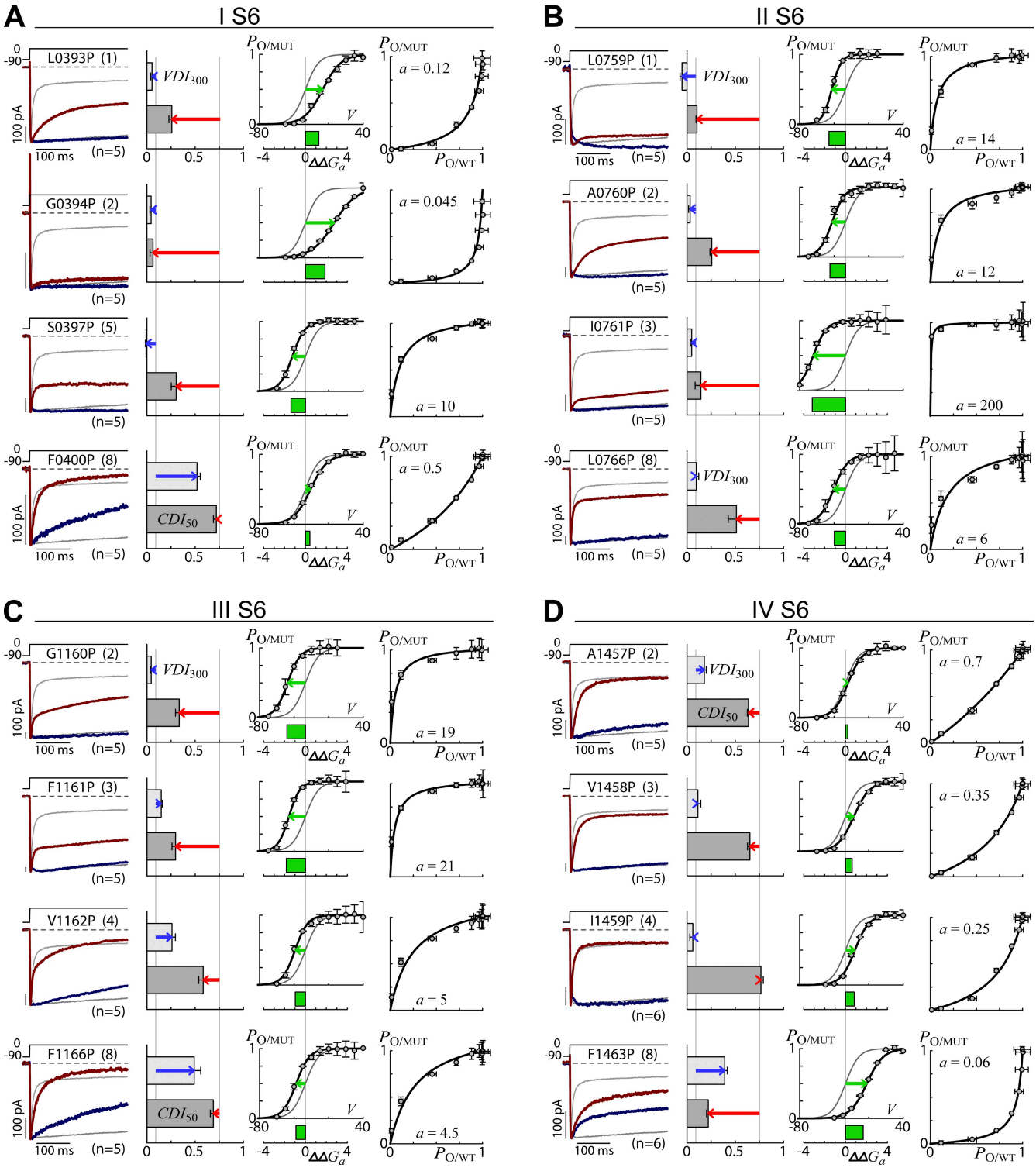

Figure 3. Functional profiles for systematic S6 mutagenesis scan. (A–D) Data are organized into four panels, where each panel corresponds to a channel domain (IS6, IIS6, IIIS6, and IVS6). Within a panel, each row corresponds to data from a $Ca_V1.3$ proline mutant coexpressed with $\alpha_2\delta$ and β_{2a}. The format for each construct follows that in Fig. 2. For clarity, only a subset of our mutagenesis screen is displayed. The complete set of S6 mutations is numerically summarized in Table II and graphically displayed in Fig. S1. Exemplar traces (left column) show Ba^{2+} (blue) and Ca^{2+} (red) currents for the mutant channel, with the native channel behavior overlaid in light gray for reference. Voltage pulse protocol and mutated residue (identified by name and common S6 coordinate, as defined in Fig. 1 A) are indicated above data traces. For *VDI* and *CDI* metrics (second column), native channel values are indicated by the vertical gray lines, and deviation from native channel behavior is indicated by colored arrows. This is also done for the voltage-activation relations (third column), which show both $\Delta\Delta G_a$ (bars) and $\Delta V_{1/2}$ (arrows). The fourth column shows fits for $\Delta\Delta G_a$ determination, as done in Fig. 2 E (left). Axis labels are shown only for top and bottom rows, with identical format throughout.

seemed to segregate among the four domains: mutations in domains II and III invariably enhanced channel activation ($\Delta\Delta G_a < 0$), mutations to domain IV almost always suppressed activation ($\Delta\Delta G_a > 0$), and mutations to domain I could produce either effect. Second, several mutations dramatically perturbed CDI, nearly eliminating CDI in some cases (e.g., Fig. 3, A, G0394P, and B, L0759P and I0761P). Finally, changes in VDI were clustered toward the distal intracellular segments of domains I, III, and IV at sites clearly distinct from those producing CDI alterations.

Mechanistic implications of interrelations between CDI and $\Delta\Delta G_a$

Does this rich assortment of functional effects (Fig. 3) adhere to a coherent pattern, distinctive of a particular end-stage inactivation mechanism (Fig. 1, C–F)? Remarkably, CDI exhibited a telling dependence on $\Delta\Delta G_a$ (Fig. 4 A), with striking correspondence to the predicted outcome for an allosteric CDI mechanism (solid curve corresponding to Eq. 5). Mutations that enhanced activation ($\Delta\Delta G_a < 0$) proportionally diminished CDI, in good agreement with the ideal relation for allosteric inhibition

TABLE II

Summary of experimental data from our mutagenesis screen

	pos	$V_{1/2}$	a	$\Delta V_{1/2}$	$\Delta\Delta G_a$	VDI_{50}	VDI_{300}	CDI_{50}	CDI_{300}	Figure
WT		−26.8	1	0.0	0.00	0.022 ± 0.006	0.091 ± 0.032	0.75 ± 0.03	0.80 ± 0.03	4 A (*i*)
G0384P	−8	−10.1	0.18	16.7	1.03	0.029 ± 0.006	0.081 ± 0.033	0.59 ± 0.04	0.73 ± 0.03	4 A (*i*)
L0393P	1	−6.7	0.12	20.1	1.27	0.021 ± 0.005	0.054 ± 0.014	0.26 ± 0.03	0.50 ± 0.03	4 B (*i*)
G0394P	2	6.5	0.045	33.4	1.86	0.033 ± 0.011	0.044 ± 0.013	0.06 ± 0.03	0.10 ± 0.03	4 B (*i*)
V0395P	3	−7.9	0.07	19.0	1.60	0.042 ± 0.015	0.147 ± 0.053	0.76 ± 0.03	0.84 ± 0.01	4 A (*ii*)
L0396P	4	−33.2	2.5	−6.3	−0.55	0.054 ± 0.012	0.207 ± 0.038	0.78 ± 0.02	0.85 ± 0.02	4 A (*ii*)
S0397P	5	−42.0	10	−15.2	−1.38	0.003 ± 0.001	−0.008 ± 0.008	0.30 ± 0.05	0.33 ± 0.06	4 A (*i*)
G0398P	6	−16.2	0.25	10.6	0.83	0.011 ± 0.008	0.064 ± 0.044	0.75 ± 0.03	0.83 ± 0.02	4 A (*i*)
E0399P	7	−25.3	0.8	1.5	0.13	0.117 ± 0.020	0.402 ± 0.025	0.79 ± 0.01	0.85 ± 0.01	4 A (*ii*)
F0400P	8	−20.9	0.5	6.0	0.42	0.159 ± 0.015	0.519 ± 0.035	0.72 ± 0.03	0.84 ± 0.03	4 A (*ii*)
L0759P	1	−42.8	14	−15.9	−1.58	0.004 ± 0.003	−0.051 ± 0.021	0.10 ± 0.01	0.18 ± 0.02	4 A (*i*)
A0760P	2	−42.3	12	−15.5	−1.49	0.005 ± 0.001	0.032 ± 0.015	0.26 ± 0.02	0.48 ± 0.01	4 A (*i*)
I0761P	3	−64.2	200	−37.4	−3.18	0.008 ± 0.001	0.048 ± 0.007	0.14 ± 0.06	0.21 ± 0.07	4 A (*i*)
A0762P	4	−47.7	15	−20.9	−1.62	0.011 ± 0.002	−0.001 ± 0.023	0.17 ± 0.06	0.22 ± 0.06	4 A (*i*)
V0763P	5	−57.1	20	−30.3	−1.80	0.008 ± 0.002	0.027 ± 0.008	0.31 ± 0.03	0.40 ± 0.03	4 A (*i*)
D0764P	6	−36.8	5	−10.0	−0.97	0.019 ± 0.011	0.085 ± 0.033	0.26 ± 0.03	0.44 ± 0.04	4 A (*i*)
N0765P	7	−44.5	11	−17.6	−1.44	0.014 ± 0.006	0.089 ± 0.028	0.42 ± 0.01	0.56 ± 0.01	4 A (*i*)
L0766P	8	−40.6	6	−13.7	−1.08	0.022 ± 0.005	0.097 ± 0.024	0.51 ± 0.08	0.57 ± 0.07	4 A (*i*)
V1159P	1	−31.2	2	−4.4	−0.42	0.010 ± 0.002	0.032 ± 0.009	0.54 ± 0.01	0.58 ± 0.01	4 A (*i*)
G1160P	2	−47.5	19	−20.7	−1.77	0.014 ± 0.003	0.045 ± 0.011	0.34 ± 0.04	0.55 ± 0.05	4 A (*i*)
F1161P	3	−45.9	21	−19.1	−1.83	0.020 ± 0.008	0.148 ± 0.012	0.30 ± 0.04	0.37 ± 0.04	4 A (*i*)
V1162P	4	−38.8	5	−12.0	−0.97	0.068 ± 0.020	0.260 ± 0.036	0.58 ± 0.05	0.83 ± 0.04	4 A (*iii*)
I1163P	5	−46.1	23	−19.3	−1.88	0.035 ± 0.008	0.119 ± 0.015	0.11 ± 0.02	0.30 ± 0.03	4 A (*i*)
V1164P	6	−50.7	48	−23.8	−2.32	0.016 ± 0.007	0.070 ± 0.011	0.20 ± 0.05	0.33 ± 0.04	4 A (*i*)
T1165P	7	−51.7	100	−24.9	−2.76	0.021 ± 0.014	0.058 ± 0.011	0.27 ± 0.04	0.60 ± 0.06	4 A (*i*)
F1166P	8	−37.5	4.5	−10.7	−0.90	0.120 ± 0.027	0.490 ± 0.067	0.69 ± 0.03	0.89 ± 0.01	4 A (*ii*)
V1456P	1	−13.2	0.12	13.7	1.27	0.032 ± 0.008	0.111 ± 0.037	0.71 ± 0.02	0.73 ± 0.01	4 A (*i*)
A1457P	2	−23.8	0.7	3.0	0.21	0.039 ± 0.010	0.179 ± 0.021	0.64 ± 0.01	0.76 ± 0.01	4 A (*iii*)
V1458P	3	−17.2	0.35	9.6	0.63	0.029 ± 0.013	0.112 ± 0.031	0.65 ± 0.02	0.74 ± 0.02	4 A (*i*)
I1459P	4	−15.9	0.25	10.9	0.83	0.011 ± 0.003	0.060 ± 0.031	0.77 ± 0.02	0.80 ± 0.02	4 A (*i*)
M1460P	5	−13.4	0.22	13.4	0.91	0.012 ± 0.002	0.027 ± 0.045	0.41 ± 0.02	0.58 ± 0.01	4 B (*i*)
D1461P	6	−25.2	0.85	1.6	0.10	0.038 ± 0.006	0.130 ± 0.014	0.67 ± 0.03	0.74 ± 0.02	4 A (*i*)
N1462P	7	−31.4	2	−4.5	−0.42	0.009 ± 0.002	0.042 ± 0.016	0.53 ± 0.02	0.55 ± 0.02	4 A (*i*)
F1463P	8	−2.2	0.06	24.7	1.69	0.256 ± 0.014	0.391 ± 0.027	0.22 ± 0.02	0.38 ± 0.03	4 B (*iii*)
D1464P	9	−7.7	0.09	19.1	1.44	0.125 ± 0.019	0.464 ± 0.031	0.68 ± 0.03	0.75 ± 0.05	4 A (*ii*)
WT/BayK		−39.2	6.5	−12.4	−1.12	0.022 ± 0.006	0.140 ± 0.038	0.46 ± 0.06	0.62 ± 0.03	5 B
V0395P/BayK	3	−14.1	0.15	12.7	1.14	0.007 ± 0.003	0.106 ± 0.032	0.78 ± 0.02	0.80 ± 0.02	5 B
N0765P/BayK	7	−56.0	125	−29.2	−2.90	0.010 ± 0.004	0.021 ± 0.011	0.12 ± 0.01	0.31 ± 0.03	5 B
V1162P/BayK	4	−37.4	5	−10.6	−0.97	0.022 ± 0.008	0.183 ± 0.046	0.62 ± 0.03	0.81 ± 0.03	5 B

Each mutant is specified by name (first column) and position (second column, corresponding to S6 coordinate in Fig. 1 A). Parameters are as defined in Table I. VDI and CDI metrics are mean ± SEM. The final column indicates the figure in which the data are plotted (Figs. 4 A, 4 B, or 5 B), followed by the corresponding zone (*i*, *ii*, or *iii*) in Fig. 5 C.

(solid curve). As for mutations that favored the closed conformation ($\Delta\Delta G_a > 0$), most (11 of 15) fit well to the top of the predicted, bell-shaped relation. Indeed, only four constructs deviated below the idealized relation for allosteric inactivation (Fig. 4 B). Closer inspection of the outlier that deviated most from theory revealed unusually large gating currents relative to ionic currents (Fig. 4 C, right, G0394P). The other three outliers also had pronounced gating currents (Fig. 4 C). In contrast, gating currents were too small to resolve in the wild-type $Ca_V1.3$ channel (Fig. 4 C, left) as well as all other mutant channels. For example, V0395P has a similar $\Delta\Delta G_a$ to the outliers, yet it has unresolvable gating current (Fig. 4 C) and resides close to the theoretical ideal (Fig. 4 A). The increased gating current in the outliers suggests that these mutations not only shift $V_{1/2}$ to the right, but also markedly suppress maximum channel open probability (Agler et al., 2005). Such pronounced dual effects in outlier channels would cause their P_O to fall well below those estimated from our convenient whole cell estimation of

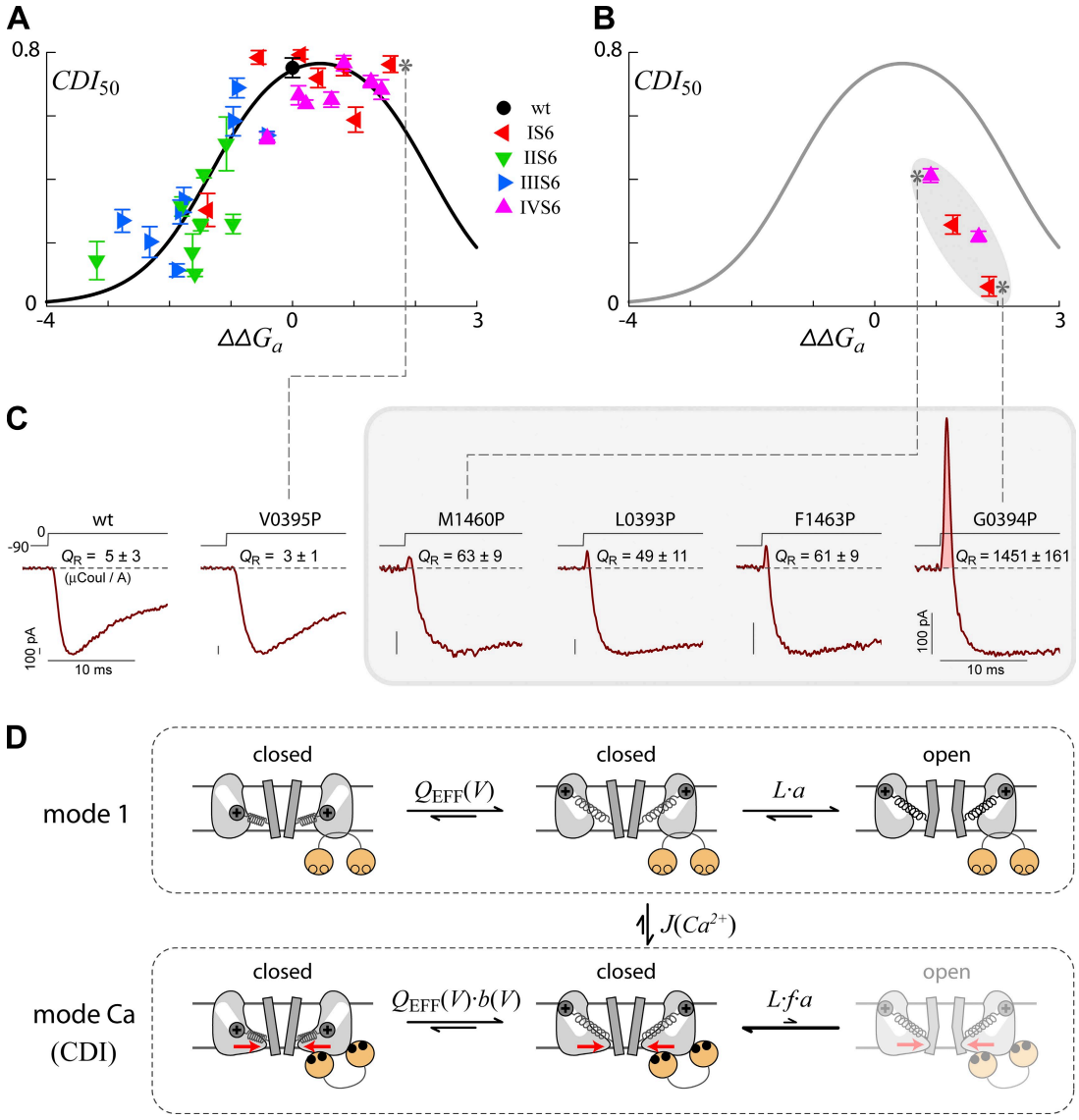

Figure 4. Implications of S6 mutagenesis scan for endpoint mechanism of CDI. (A and B) CDI_{50} versus $\Delta\Delta G_a$ for our $Ca_V1.3$ mutant library. Symbol color and shape as in legend. Error bars are SEM. Overlaid are the model results identical to Fig. 1 F. (C) Gating currents of channels that fall on (left) and off (right, gray shaded) the predicted CDI-$\Delta\Delta G_a$ relation. Q_R is the ratio of gating current area (e.g., pink shaded area of G0394P) to peak ionic current (units of μCoul/A). The mean ± SEM is shown for each construct. (D) CDI occurs via an allosteric mechanism. Channels occupy either a normal (top row) or inactivated gating mode (bottom row). In either mode, channel activation begins with voltage sensor (+) movement (governed by $Q_{EFF}(V)$) and ends with S6 gate opening (governed by L). Outward voltage sensor displacement promotes S6 gate opening (depicted with springs). CaM (yellow dumbbell) binds Ca^{2+} (black dots in bottom row) and initiates CDI by interacting with a channel site distinct from the S6 gate. This causes a conformational change (red arrows) that inhibits S6 gate opening (i.e., parameter $f < 1$). Thus, voltage and Ca^{2+} ultimately exert opposing actions on the same S6 gate.

$P_O(V)$ relations (Fig. 2, C and D). This unaccounted-for decrease in P_O would produce smaller F_{CDI} values than predicted by Eq. 4 (dotted curve in Fig. 1 F), yielding the observed deviation from ideality in Fig. 4 B. Although the whole cell estimation of $P_O(V)$ relations lacks the single-channel resolution needed to directly account for changes in maximum open probability (Tadross et al., 2008), the close correspondence of the vast majority of mutants (30 of 34) to the ideal relation in Fig. 4 A suggests that mutation-induced effects on maximum channel open probability are minimal in the majority of cases. This ultimate result, combined with the need for technical simplicity in a mutagenesis screen of this magnitude, validates the simple whole cell approach.

Bay K 8644 effects cohere to the same *CDI*-$\Delta\Delta G_a$ relation

To confirm the generality of the allosteric relation in Fig. 4 A, we tested the effects of Bay K 8644, a well-known pharmacological agent that interacts with S5/S6 regions to enhance channel opening, i.e., to decrease $\Delta\Delta G_a$ (Grabner et al., 1996). Fig. 5 A (top) shows the behavior of $Ca_V1.3$ in the presence of 5 µM Bay K 8644. As expected, there is a marked hyperpolarizing shift of the activation curve ($\Delta\Delta G_a < 0$). Interestingly, CDI diminishes appreciably, and by an extent that accords precisely with our established relation (Fig. 5 B, black symbols). Similarly, the addition of Bay K 8644 to a left-shifted II-S6 mutant (N0765P) markedly enhances activation and nearly eliminates CDI (Fig. 5 A, middle), also in agreement with the allosteric prediction (Fig. 5 B, green symbols). To exclude nonspecific effects, adding Bay K 8644 to a right-shifted I-S6 mutant (V0395P) enhances activation, yet has little effect on CDI (Fig. 5, A, bottom, and B, red symbols). Finally, Bay K 8644 has no effect on activation or CDI of a III-S6 mutant (Fig. 5 B, blue symbols, V1162P), consistent with prior work in $Ca_V1.2$ identifying III-S6 as a drug-binding site (Grabner et al., 1996). Remarkably, Bay K 8644 alters CDI mainly insofar as it boosts activation (Fig. 5 B), without further indiscriminate effects.

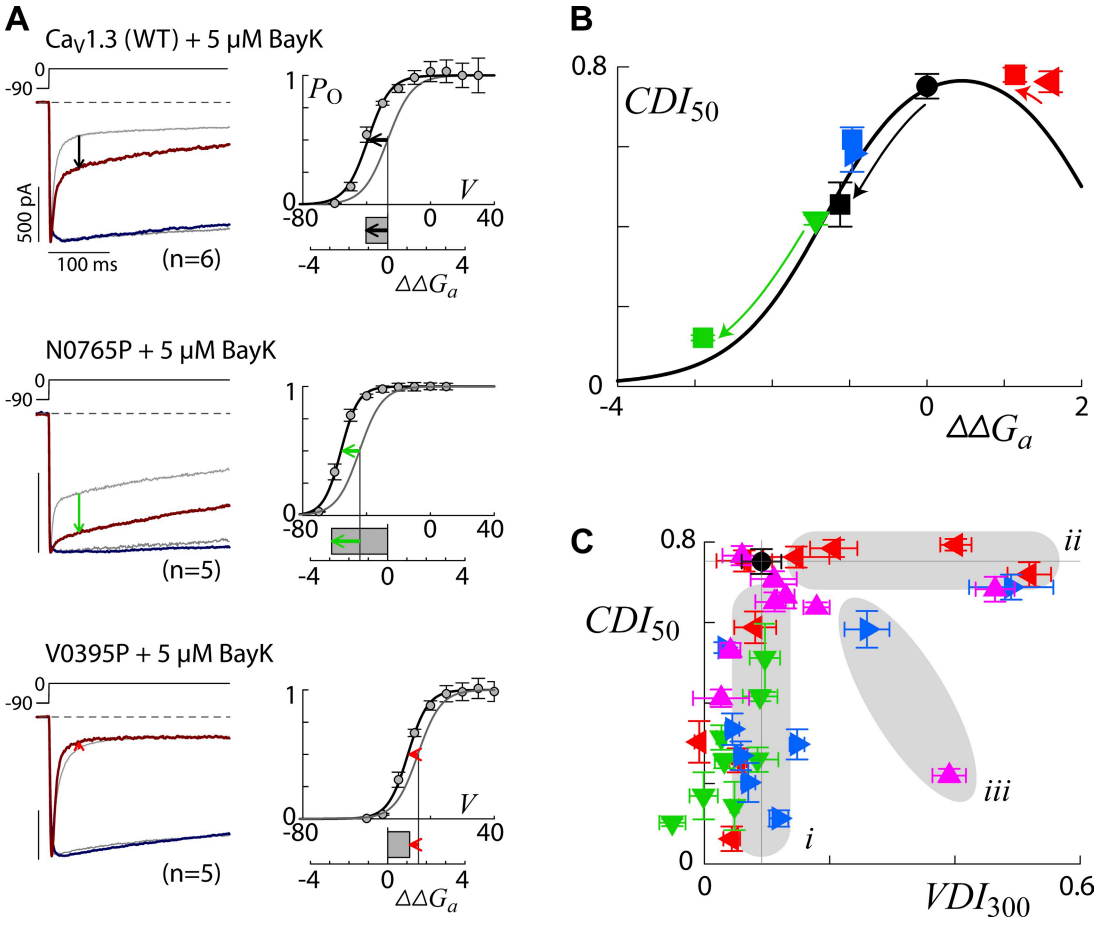

Figure 5. Further implications of S6 mutagenesis scan for endpoint mechanism of CDI. (A) Behavior of wild-type $Ca_V1.3$ (top row), N0765P (middle), and V0395P (bottom) channels coexpressed with $\alpha_2\delta$ and β_{2a} in 5 µM Bay K 8644. Gray traces show corresponding drug-free behavior. Colored arrows indicate change resulting from Bay K. (B) CDI_{50} versus $\Delta\Delta G_a$ of wild-type $Ca_V1.3$ (black symbols), N0765P (green symbols), V0395P (red symbols), and V1162P (blue symbols); each construct is plotted both in the absence (circle or triangles) and presence (squares) of Bay K. (C) CDI_{50} versus VDI_{300} for our $Ca_V1.3$ mutant library. Symbol color and shape as in Fig. 4 A. Data are clustered into three main zones, which are discussed in the Results.

VDI involves a "hinged lid–shield" mechanism in $Ca_V1.3$

Our S6 mutations affected VDI in very different ways, demonstrating that VDI and CDI are distinctly different processes. This contrasting behavior is highlighted in Fig. 5 C (also see Table II), which plots CDI versus VDI for our entire library of mutants. Most of the time, significant effects on CDI occur with relatively minor changes in VDI (zone *i*). When changes in VDI do occur, CDI is either unperturbed (zone *ii*) or perturbed in the opposite direction (zone *iii*). The latter discordance is particularly striking for the F1463P mutant. Here, CDI sharply decreases, yet VDI strongly intensifies (Figs. 5 C and 3 D).

Beyond this fundamental difference, we identified two mechanistically telling patterns of VDI effects. First, mutations producing the greatest alteration in VDI all cluster at the very distal ends of S6 segments, as seen by mapping VDI_{300} onto our structural homology model (Fig. 6 A). In particular, these VDI "hotspots" (red) reside entirely below the putative bundle crossing (arrow). Second, mutations at VDI hotspots invariably increase the extent of inactivation. In contrast, nearly all prior S6 mutations (all in $Ca_V1.2$ and $Ca_V2.1$) produced decreases in VDI at residues above the putative bundle crossing (Kraus et al., 1998, 2000; Stotz et al., 2000, 2004; Stotz and Zamponi, 2001; Splawski et al., 2004, 2005; Hoda et al., 2005; Hohaus et al., 2005; Raybaud et al., 2006, 2007; Barrett and Tsien, 2008). These residues have been proposed as the "receptor" for a hinged lid.

These two discrepancies from prior patterns hint at a unique mechanism of VDI in $Ca_V1.3$. To start, the distal location of hotspot residues might initially suggest that these residues comprise part of a hinged-lid receptor site, with a different location than that found in $Ca_V1.2$ channels. However, the increase rather than decrease in VDI caused by these hotspot mutations argues against this notion, for it is implausible that proline mutations would generate de novo functionality, such as enhanced VDI. Instead, these hotspot residues might comprise part of an element that prevents VDI in $Ca_V1.3$ channels, i.e., something akin to a shield (Fig. 6 B, red) that prevents a hinged lid–like module (blue) from reaching its S6 binding site (green). The distal S6 mutations might have disrupted this shield, thus promoting VDI (Fig. 6 C).

If so, one might expect $Ca_V1.3$ channels to be insensitive to perturbations of the presumed hinged lid itself because the shield would block the lid regardless of its properties. One test of this prediction comes with the use of different auxiliary β subunits, all of which bind the presumed hinged lid comprised of the intracellular loop between channel domains I and II ("I-II loop"). The prevailing view in most Ca^{2+} channels is that the β_{2a} subunit is palmitoylated and anchored to the membrane (Fig. 6 D, top left), thereby restricting lid mobility and diminishing VDI. In contrast, the β_{1b} subunit lacks such palmitoylation (Fig. 6 D, bottom left) and VDI becomes much faster. However, according to the shield hypothesis, VDI of $Ca_V1.3$ channels should be insensitive to the type of β subunit. In fact, both the wild-type $Ca_V1.3$ and a non-hotspot mutant (N1462P) exhibit identically weak VDI with either β_{2a} or β_{1b} (Fig. 6 D) (Shen et al., 2006). This outcome is unique to $Ca_V1.3$, as the switch from β_{2a} to β_{1b} significantly accelerates VDI in nearly all other $Ca_V1/2$ channels (Jones et al., 1998; Bourinet et al., 1999; Stotz et al., 2000, 2004; Bernatchez et al., 2001; Stotz and Zamponi, 2001; Dafi et al., 2004). A more stringent test concerns the effects of different β subunits if the presumed shield were first disrupted. In this context, VDI should then become sensitive to the type of β subunit. Indeed, when the presumed shield is eliminated with either of two VDI hotspot mutations, switching from β_{2a} to β_{1b} causes a marked acceleration of VDI (Fig. 6 E). In all, the data thus far argues well for the existence of a shield against VDI.

Still needed, however, is direct evidence that the basic hinged-lid mechanism identified in $Ca_V1.2$ channels is retained in $Ca_V1.3$. Notably, for more proximal S6 residues identified in $Ca_V1.2$ as critical to a hinged-lid receptor site (Hohaus et al., 2005), our own $Ca_V1.3$ mutations at the analogous residues exhibit VDI no different than that observed at baseline in Fig. 7 A. This lack of effect could be rationalized by supposing that the $Ca_V1.3$ receptor site is shielded from the hinged lid so receptor disruption would have no appreciable effect on VDI (Fig. 7 B). To test directly for a hinged-lid mechanism in $Ca_V1.3$, it would be necessary to first disrupt the shield, e.g., with an initial D1464P mutation (Fig. 7, C and D). Given this starting point, additional mutations at positions homologous to hinged-lid receptor sites in $Ca_V1.2$ should diminish VDI. The rapid VDI seen upon shield disruption gives the baseline against which further mutations will be compared (Fig. 7 C). Reassuringly and without exception, additional mutations at homologous hinged-lid receptor sites now produce a striking slowing of VDI (Fig. 7, E and F). The G398P mutation in IS6 is analogous to the $Ca_V1.2$ G406R mutation that underlies forms of Timothy syndrome (Splawski et al., 2004, 2005; Barrett and Tsien, 2008), and the L0759 and A0760 mutations in IIS6 correspond to rabbit $Ca_V1.2$ receptor sites at L0779 and A0780 (Hohaus et al., 2005). These results furnish strong evidence that these residues contribute to a hinged-lid receptor, analogous to that described in $Ca_V1.2$.

DISCUSSION

CaM-mediated inactivation may act by allosteric inhibition of activation gate

The past decade has witnessed many discoveries about the early events underlying Ca^{2+}/CaM modulation of the family of Ca^{2+} channels. Much is now known about the positioning of Ca^{2+}-free CaM (apoCaM) on the channel, the binding of Ca^{2+} to this "pre-associated" CaM, and the initial Ca^{2+}/CaM interaction sites on the channel (Dunlap, 2007).

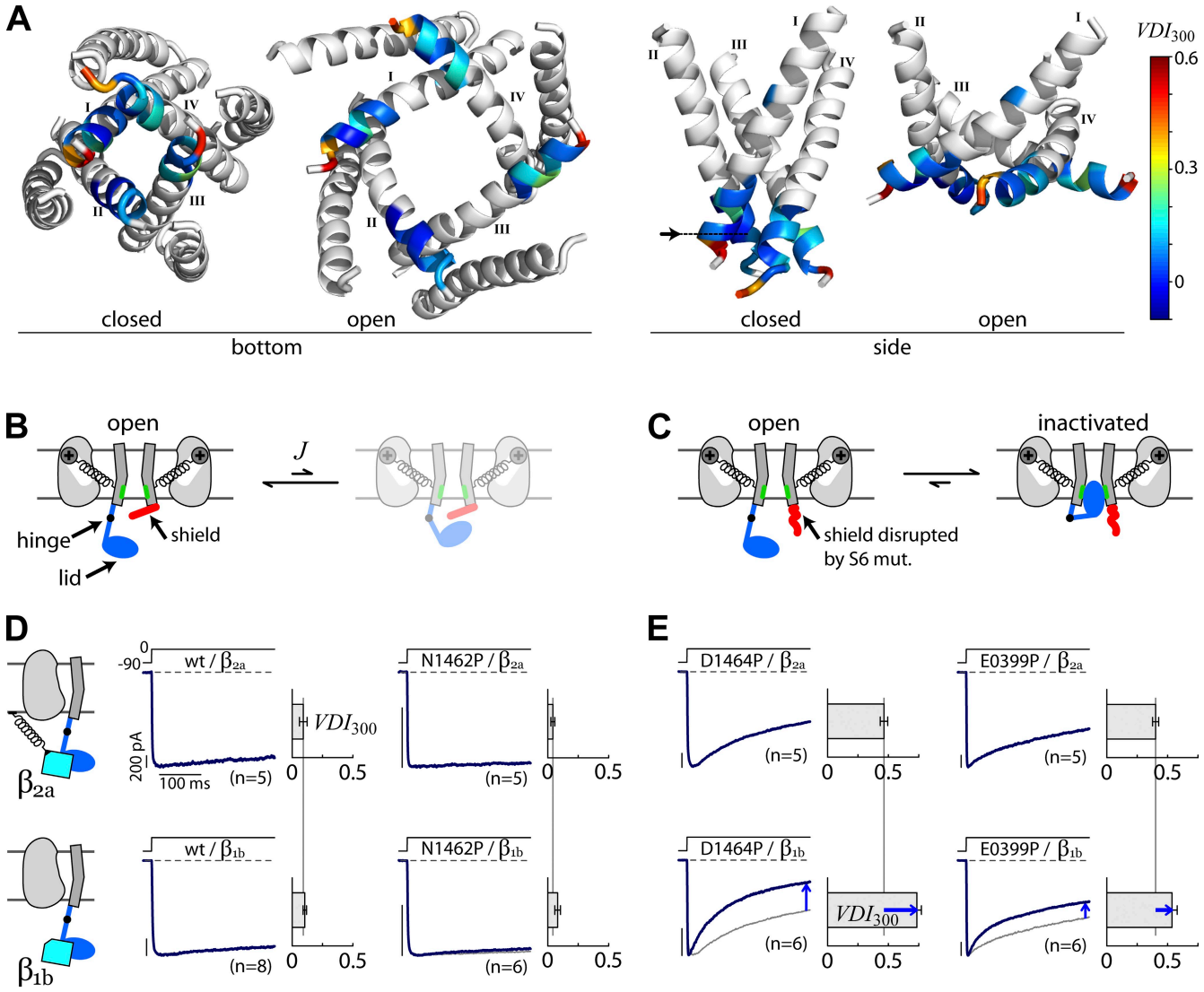

Figure 6. Mechanistic insights for VDI. (A) VDI perturbations mapped onto the $Ca_V1.3$ homology model from Fig. 1 B. Residues outside of mutagenesis screen shown in gray. Colored regions indicate VDI_{300} upon mutation to proline. See color legend to right, and note that native channel VDI_{300} is ~0.1 (blue). (B and C) Proposed mechanism of VDI in $Ca_V1.3$. Native channels (B) have very little VDI, likely due to the presence of a shield (red), which prevents the hinged lid (blue) from reaching its binding site (green). VDI-enhancing S6 mutations likely disrupt this shield (C). (D and E) Sensitivity of VDI to β subunits supports the notion of a shield in $Ca_V1.3$. Although β_{1b} typically enhances VDI by allowing greater hinged-lid mobility than β_{2a} (cartoon in D), native $Ca_V1.3$ and non-hotspot mutant N1462P have no such effect (D). In contrast, if the putative shield is perturbed (two mutants in E), β_{1b} significantly enhances VDI.

In contrast, the ensuing movements of cytoplasmic loops and the eventual actions that produce channel inactivation (or facilitation) have remained largely unknown. This paper furnishes new evidence that allosteric inhibition of the activation gate is the ultimate outcome for the CaM-mediated CDI of $Ca_V1.3$ channels. A like hypothesis was proposed for $Ca_V1.2$, based on single-channel recordings (Imredy and Yue, 1994). Here, our present work transforms this suggestion into an explicit mechanism, key features of which are illustrated in Fig. 4 D.

First, just as voltage depolarization can enhance opening of the S6 activation gate (Fig. 4 D, springs), CaM-driven conformational changes act to suppress opening of the very same cytoplasmic gate (red arrows in bottom row). Thus, CDI corresponds to an inactivated gating mode ("mode Ca") in which channels open sparsely due to an increase in the chemical energy needed to open the S6 gate ($f < 1$ in the bottom row). Interestingly, a simple variant of this allosteric mechanism, with $f > 1$, could explain CaM-induced facilitation in $Ca_V2.1$ channels (Chaudhuri et al., 2007).

Second, other features of our results generalize key principles of channel activation across the superfamily of voltage-gated channels. Notably, our data support the principle of separability between the initial movements of voltage-sensing domains (via $Q_{EFF}(V)$) and the subsequent

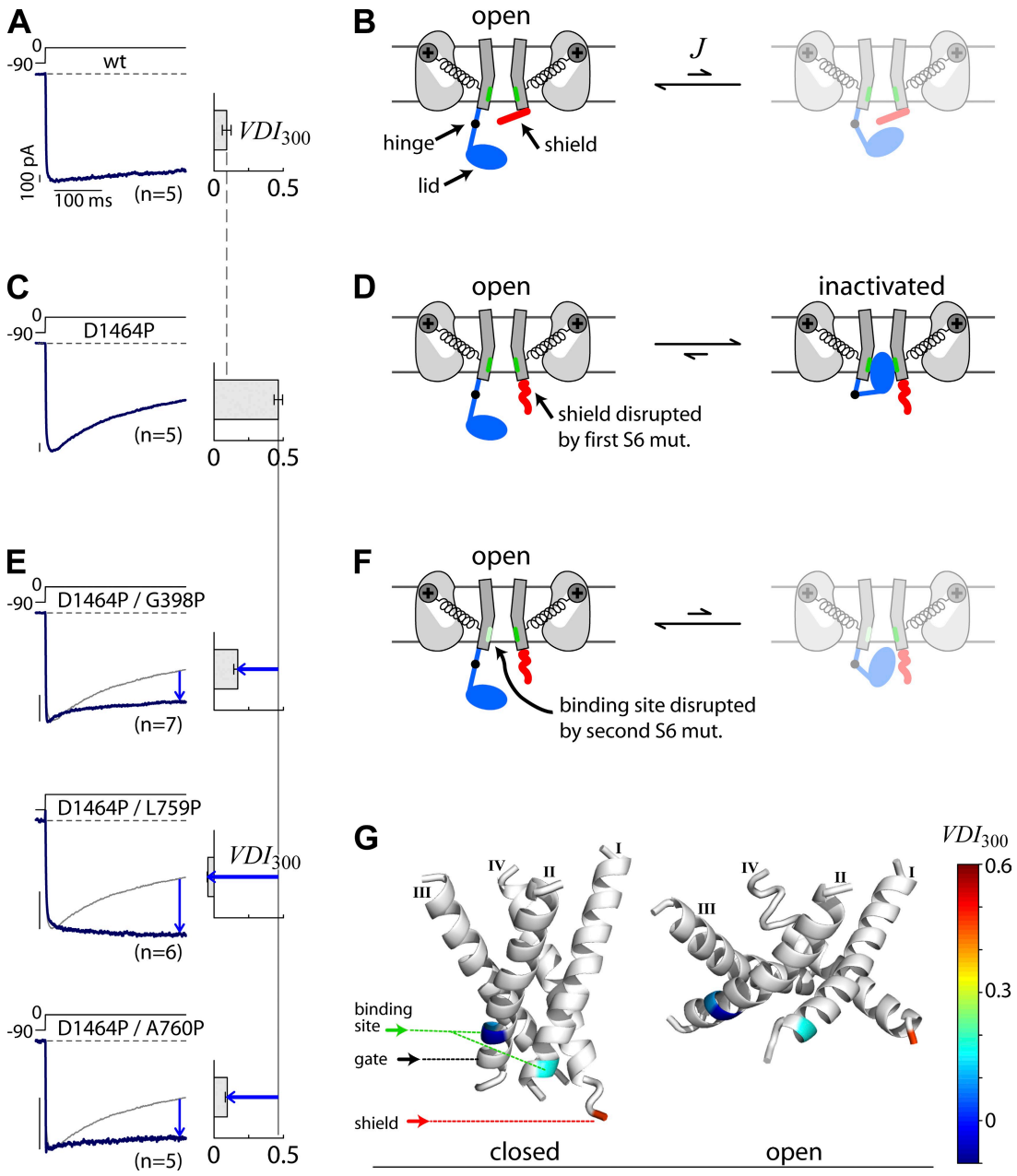

Figure 7. Further mechanistic insights for VDI. (A–D) Review of proposed shield structure. In A and B, native $Ca_V1.3$ channels have very little VDI, likely due to the presence of a shield (red) that prevents the hinged lid (blue) from reaching its binding site (green). Conversely, in C and D, shield-disrupting mutation D1464P enhances VDI, even when coexpressed with $\alpha_2\delta$ and β_{2a}, here and subsequently. (E and F) Evidence that an underlying hinged-lid mechanism exists in $Ca_V1.3$. Given a baseline shield-disrupting D1464P mutation, additional mutations at sites homologous to those previously identified as a hinged-lid binding site (green) significantly diminish VDI. The G398P mutation is analogous to the $Ca_V1.2$ G406R mutation that underlies forms of Timothy syndrome, and the L0759P and A0760P mutations in IIS6 correspond to rabbit $Ca_V1.2$ receptor sites at L0779 and A0780. (G) Structural model of components underlying the hinged lid–shield mechanism. VDI for the constructs in C and E are mapped onto our $Ca_V1.3$ homology model. The pronounced VDI of D1464P (red residue) indicates the shield location below the putative gate (identified by black arrow). The loss of this VDI upon mutation of additional residues (blue and cyan) identifies the location of the proposed hinged-lid binding site (identified by green arrow) above the gate. These binding site residues move considerably in the open versus closed conformations, consistent with preferential open-state accessibility.

opening of the cytoplasmic activation gate (via L, shown explicitly as two separate transitions in Fig. 4 D), a theme with considerable support in voltage-gated K^+ channels (Zagotta et al., 1994; Yifrach and MacKinnon, 2002). In the Ca^{2+} channel case, this view is reinforced by the analysis used to determine $\Delta\Delta G_a$ (Eq. 6 and Fig. 2 E), which tests the separability of voltage sensing (via $Q_{EFF}(V)$) and subsequent opening of the S6 gate (via L). Only 2 of 34 mutations had $P_{O/MUT}$–$P_{O/WT}$ relations that could not be fit with Eq. 6 (A0762P and V0763P in

Fig. S1), indicating that $Q_{EFF}(V)$ changed in these rare cases. For the vast majority of mutants, the close correspondence of data to Eq. 6 (Fig. 3, right columns, and Fig. S1, right columns) supports the notion that S6 mutations do not, in general, alter voltage sensing ($Q_{EFF}(V)$ unchanged in Fig. 4 D) despite marked changes in the subsequent opening step ($a \neq 1$). This result empirically substantiates the use of proline substitutions in our screen. Interestingly, the atypical residues in $Ca_V1.3$ that seem to alter voltage sensing upon mutation to proline correspond to a closely homologous region in $Ca_V1.2$, where an A780P mutation (analogous to A0760P in the present study) was believed to disturb voltage sensor function (Beyl et al., 2009), suggesting conserved structural underpinnings across the Ca_V1 family. Another key principle concerns the concerted nature of the final S6 gate opening, where an alteration to any individual S6 segment would affect the combined movement of all four elements (Yifrach and MacKinnon, 2002). This is supported by the finding that widely dispersed S6 mutations in all four domains exert strong effects on activation (Fig. 3). In contrast, some prior studies have suggested that Ca^{2+} channel opening is dominated by a glycine hinge (GX9GX3G) in IS6 (Raybaud et al., 2006). Here, we find that although mutations of these glycines do alter activation, manipulations at many other sites have significantly stronger effects.

Finally, our new results about the end-stage effects of CDI, together with rapid advances concerning the early events underlying Ca^{2+}/CaM modulation of $Ca_V1/2$ channels, set the stage for investigating the events that link these two realms. In this regard, it may be relevant that a recent elegant study finds that CDI is diminished by introducing glycines just downstream of the IS6 region in $Ca_V1.2$ channels (Findeisen and Minor, 2009). Perhaps this region couples cytoplasmic CaM-mediated torque to IS6 gating elements. Similarly, it will be interesting if analogous regions in other homologous domains prove equally important for CDI. In all, answering how the CaM/IQ domain communicates allosterically with the S6 gate now looms as a critical and open question in the field.

VDI may involve a hinged lid–shield mechanism in $Ca_V1.3$

Although our library of S6 mutations has strong effects on both VDI and CDI, the pattern of effects is entirely different for these two forms of inactivation (Fig. 5 C). Thus, a common structural component (the S6 gate) may play a role in gating processes that are nonetheless functionally distinct. For CDI, S6 mutations are notable for altering the propensity to open, which through allosteric coupling change the strength of inactivation. For VDI, S6 mutations appear important for disrupting either a shield or receptor for a hinged lid.

Beyond the separate nature of VDI and CDI, our data support the existence of a $Ca_V1.3$ hinged lid–shield VDI mechanism, which represents an important variant of the hinged-lid process proposed in $Ca_V1.2$ and Ca_V2 channels (Hohaus et al., 2005; Evans and Zamponi, 2006). Importantly, we believe that the underlying hinged-lid mechanism in $Ca_V1.3$ could not be immediately discerned in wild-type channels because of the existence of a shield that repels lid closure (Fig. 7, A and B). Only after the introduction of shield-disrupting mutations do the hallmarks of a hinged-lid mechanism emerge in the $Ca_V1.3$ context. In particular, shield disruption produces both VDI sensitivity to the identity of the β subunit (Fig. 6 E) and a slowing of VDI upon additional mutation at residues comprising the presumed hinged-lid receptor (Fig. 7 E). Fig. 7 G summarizes the structural components underlying the proposed hinged lid–shield mechanism. Of note, shield residues (red) fall below the putative gate location (identified by black arrow), whereas binding site residues (blue and cyan) sit above the gate. These binding site residues move considerably in the open versus closed conformations (Fig. 7 G), consistent with preferential open-state accessibility (Tadross and Yue, 2010). The shield, which seems to be a unique specialization in $Ca_V1.3$ channels, may play a fundamental role in ribbon synapses of the eye and ear, where $Ca_V1.3$ channels must maintain channel opening despite prolonged activation (Yang et al., 2006).

Given a recent hypothesis (Findeisen and Minor, 2009), our findings merit further comment regarding the interrelation between VDI and the I-II loop between homologous domains I and II. This loop contains an 18-residue helical segment called the AID, which interacts with the auxiliary β subunit of Ca^{2+} channels (Chen et al., 2004; Opatowsky et al., 2004; Van Petegem et al., 2004). One face of the AID is hydrophobic and binds to the β subunit. Residues of the opposite hydrophilic face of the AID have been shown to play a critical role in VDI, consistent with the notion that the β–AID complex is the "lid" that binds to S6 residues and occludes the pore in VDI (Dafi et al., 2004). In contrast, a more recent study models the residues upstream of the AID region (the IS6-AID linker) as an invariably rigid helical segment (Vitko et al., 2008) that positions the β–AID complex at a significant distance from the channel pore—too far away to bind or occlude the S6 gate (Findeisen and Minor, 2009). This structural model was taken as evidence against a hinged-lid mechanism involving the I-II loop (Findeisen and Minor, 2009). Although a strictly rigid IS6-AID linker would prevent β–AID occlusion of the pore, the apparent controversy could be reconciled if the IS6-AID linker were, under some conditions, to bend and function as a "hinge" (Fig. 7, B and D). No empirical data currently exclude the possibility of such dynamic bending of the IS6-AID linker. Moreover, the acceleration of VDI by the introduction of glycines into the IS6-AID linker (Findeisen and Minor, 2009) fits well with the notion of augmenting flexibility of a hinge region. Together with the new lines of evidence in this

paper, we suggest that a hinged lid–shield mechanism—where the IS6-AID linker functions as the hinge, and the downstream β–AID complex functions as the lid—remains worthy of continued investigation.

Implications for Ca^{2+} channelopathies involving S6 segments

Beyond channel mechanism, this study furnishes a unifying framework for understanding heritable diseases involving S6 mutations in both neuronal and cardiac Ca^{2+} channels (Kraus et al., 1998, 2000; Splawski et al., 2004, 2005; Hoda et al., 2005; Hohaus et al., 2005; Barrett and Tsien, 2008). The phenotypic manifestations of these diseases are diverse, including migraine, ataxia, autism, physical deformities, and cardiac arrhythmias. These are believed to result from abnormal VDI, CDI, Ca^{2+}-dependent facilitation, or some combination of these. A first insight is that, besides changes in inactivation or facilitation, these channelopathies are likely to exhibit potent alterations in open probability, and either (or both) of these effects may contribute to pathogenesis. For example, in Timothy syndrome, where the slowing of VDI by IS6 mutations in $Ca_V1.2$ has attracted the most attention (Barrett and Tsien, 2008), accompanying changes in open probability may be equally relevant (Erxleben et al., 2006). Conversely, in familial hemiplegic migraine, where the long-standing emphasis has been on altered open probability produced by S6 mutations in $Ca_V2.1$ (Cao and Tsien, 2005; Pietrobon, 2007), a recent preliminary report indicates reductions in Ca^{2+}-dependent facilitation (Adams et al., 2007). A second key insight is that VDI abnormalities in S6 channelopathies may result from direct perturbation of either the hinged-lid binding site or the newly proposed shield structure. Either of these perturbations might prove difficult to reverse pharmacologically because the fundamental VDI machinery has been compromised. In contrast, S6 channelopathies that affect CDI might be amenable to pharmaceutical intervention because the actual CDI machinery is likely intact. The apparent CDI deficit arises as an indirect result of altered channel activation (Fig. 4, A and D), something that can be readily reversed. Indeed, several compounds such as dihydropyridine agonists (e.g., Bay K 8644 in Fig. 5, A and B) and antagonists can modulate channel activation. If properly administered with sufficient selectivity, similar compounds may simultaneously normalize activation and CDI, according to the relation in Fig. 5 B. Interestingly, Bay K 8644 can recapitulate many of the cardiac features of Timothy syndrome (Sicouri et al., 2007), a $Ca_V1.2$ channelopathy involving mutations in I-S6. Additionally, recent clinical work suggests that verapamil, a Ca^{2+} channel–blocking compound, partially relieves cardiac symptoms of Timothy syndrome (Jacobs et al., 2006). In all, modulators of Ca^{2+} channel activation, fine-tuned by the principles outlined here, may ultimately prove therapeutic.

We thank Wanjun Yang for dedicated technical support and Ivy Dick for helpful comments on the manuscript.

This work was supported by a Medical Scientist Training Program fellowship of the National Institute of General Medical Sciences (to M.R. Tadross) and by grant RO1MH065531 of the National Institute of Mental Health (to D.T. Yue).

Angus C. Nairn served as editor.

Submitted: 31 July 2009
Accepted: 14 January 2010

REFERENCES

Adams, P.J., E. Garcia, T.P. Snutch, and S.D. Spacey. 2007. Splice variant composition of P/Q-type calcium channels affects both biophysical properties and sensitivity to an FHM point mutation. *Biophys. J.* Abstr 2869:602A.

Agler, H.L., J. Evans, L.H. Tay, M.J. Anderson, H.M. Colecraft, and D.T. Yue. 2005. G protein-gated inhibitory module of N-type (ca(v)2.2) ca2+ channels. *Neuron*. 46:891–904. doi:10.1016/j.neuron.2005.05.011

Armstrong, C.M., and F. Bezanilla. 1977. Inactivation of the sodium channel. II. Gating current experiments. *J. Gen. Physiol.* 70:567–590. doi:10.1085/jgp.70.5.567

Babich, O., D. Isaev, and R. Shirokov. 2005. Role of extracellular Ca2+ in gating of CaV1.2 channels. *J. Physiol.* 565:709–715. doi:10.1113/jphysiol.2005.086561

Babich, O., J. Reeves, and R. Shirokov. 2007. Block of $Ca_V1.2$ channels by Gd^{3+} reveals preopening transitions in the selectivity filter. *J. Gen. Physiol.* 129:461–475. doi:10.1085/jgp.200709733

Barrett, C.F., and R.W. Tsien. 2008. The Timothy syndrome mutation differentially affects voltage- and calcium-dependent inactivation of CaV1.2 L-type calcium channels. *Proc. Natl. Acad. Sci. USA.* 105:2157–2162. doi:10.1073/pnas.0710501105

Beedle, A.M., J. Hamid, and G.W. Zamponi. 2002. Inhibition of transiently expressed low- and high-voltage-activated calcium channels by trivalent metal cations. *J. Membr. Biol.* 187:225–238. doi:10.1007/s00232-001-0166-2

Bernatchez, G., L. Berrou, Z. Benakezouh, J. Ducay, and L. Parent. 2001. Role of Repeat I in the fast inactivation kinetics of the Ca(V)2.3 channel. *Biochim. Biophys. Acta.* 1514:217–229. doi:10.1016/S0005-2736(01)00373-X

Berridge, M.J., P. Lipp, and M.D. Bootman. 2000. The versatility and universality of calcium signalling. *Nat. Rev. Mol. Cell Biol.* 1:11–21. doi:10.1038/35036035

Beyl, S., E.N. Timin, A. Hohaus, A. Stary, M. Kudrnac, R.H. Guy, and S. Hering. 2007. Probing the architecture of an L-type calcium channel with a charged phenylalkylamine: evidence for a widely open pore and drug trapping. *J. Biol. Chem.* 282:3864–3870. doi:10.1074/jbc.M609153200

Beyl, S., P. Kügler, M. Kudrnac, A. Hohaus, S. Hering, and E. Timin. 2009. Different pathways for activation and deactivation in $Ca_V1.2$: a minimal gating model. *J. Gen. Physiol.* 134:231–241. doi:10.1085/jgp.200910272

Bourinet, E., T.W. Soong, K. Sutton, S. Slaymaker, E. Mathews, A. Monteil, G.W. Zamponi, J. Nargeot, and T.P. Snutch. 1999. Splicing of alpha 1A subunit gene generates phenotypic variants of P- and Q-type calcium channels. *Nat. Neurosci.* 2:407–415. doi:10.1038/8070

Cao, Y.Q., and R.W. Tsien. 2005. Effects of familial hemiplegic migraine type 1 mutations on neuronal P/Q-type Ca2+ channel activity and inhibitory synaptic transmission. *Proc. Natl. Acad. Sci. USA.* 102:2590–2595. doi:10.1073/pnas.0409896102

Cens, T., S. Restituito, S. Galas, and P. Charnet. 1999. Voltage and calcium use the same molecular determinants to inactivate calcium channels. *J. Biol. Chem.* 274:5483–5490. doi:10.1074/jbc.274.9.5483

Chaudhuri, D., J.B. Issa, and D.T. Yue. 2007. Elementary mechanisms producing facilitation of $Ca_V2.1$ (P/Q-type) channels. *J. Gen. Physiol.* 129:385–401. doi:10.1085/jgp.200709749

Chen, Y.H., M.H. Li, Y. Zhang, L.L. He, Y. Yamada, A. Fitzmaurice, Y. Shen, H. Zhang, L. Tong, and J. Yang. 2004. Structural basis of the alpha1-beta subunit interaction of voltage-gated Ca2+ channels. *Nature.* 429:675–680. doi:10.1038/nature02641

Choi, K.L., R.W. Aldrich, and G. Yellen. 1991. Tetraethylammonium blockade distinguishes two inactivation mechanisms in voltage-activated K+ channels. *Proc. Natl. Acad. Sci. USA.* 88:5092–5095. doi:10.1073/pnas.88.12.5092

Cordero-Morales, J.F., V. Jogini, A. Lewis, V. Vásquez, D.M. Cortes, B. Roux, and E. Perozo. 2007. Molecular driving forces determining potassium channel slow inactivation. *Nat. Struct. Mol. Biol.* 14:1062–1069. doi:10.1038/nsmb1309

Dafi, O., L. Berrou, Y. Dodier, A. Raybaud, R. Sauvé, and L. Parent. 2004. Negatively charged residues in the N-terminal of the AID helix confer slow voltage dependent inactivation gating to CaV1.2. *Biophys. J.* 87:3181–3192. doi:10.1529/biophysj.104.045559

Dick, I.E., M.R. Tadross, H. Liang, L.H. Tay, W. Yang, and D.T. Yue. 2008. A modular switch for spatial Ca^{2+} selectivity in the calmodulin regulation of Ca_V channels. *Nature.* 451:830–834. doi:10.1038/nature06529

Doyle, D.A., J. Morais Cabral, R.A. Pfuetzner, A. Kuo, J.M. Gulbis, S.L. Cohen, B.T. Chait, and R. MacKinnon. 1998. The structure of the potassium channel: molecular basis of K+ conduction and selectivity. *Science.* 280:69–77. doi:10.1126/science.280.5360.69

Dunlap, K. 2007. Calcium channels are models of self-control. *J. Gen. Physiol.* 129:379–383. doi:10.1085/jgp.200709786

Erickson, M.G., B.A. Alseikhan, B.Z. Peterson, and D.T. Yue. 2001. Preassociation of calmodulin with voltage-gated Ca(2+) channels revealed by FRET in single living cells. *Neuron.* 31:973–985. doi:10.1016/S0896-6273(01)00438-X

Erickson, M.G., H. Liang, M.X. Mori, and D.T. Yue. 2003. FRET two-hybrid mapping reveals function and location of L-type Ca2+ channel CaM preassociation. *Neuron.* 39:97–107. doi:10.1016/S0896-6273(03)00395-7

Erxleben, C., Y. Liao, S. Gentile, D. Chin, C. Gomez-Alegria, Y. Mori, L. Birnbaumer, and D.L. Armstrong. 2006. Cyclosporin and Timothy syndrome increase mode 2 gating of CaV1.2 calcium channels through aberrant phosphorylation of S6 helices. *Proc. Natl. Acad. Sci. USA.* 103:3932–3937. doi:10.1073/pnas.0511322103

Eswar, N., B. Webb, M.A. Marti-Renom, M.S. Madhusudhan, D. Eramian, M.Y. Shen, U. Pieper, and A. Sali. 2006. Comparative protein structure modeling using Modeller. *Curr. Protoc. Bioinformatics* Chaper 5:Unit 5.6.

Evans, R.M., and G.W. Zamponi. 2006. Presynaptic Ca2+ channels—integration centers for neuronal signaling pathways. *Trends Neurosci.* 29:617–624. doi:10.1016/j.tins.2006.08.006

Findeisen, F., and D.L. Minor Jr. 2009. Disruption of the IS6-AID linker affects voltage-gated calcium channel inactivation and facilitation. *J. Gen. Physiol.* 133:327–343. doi:10.1085/jgp.200810143

Grabner, M., Z. Wang, S. Hering, J. Striessnig, and H. Glossmann. 1996. Transfer of 1,4-dihydropyridine sensitivity from L-type to class A (BI) calcium channels. *Neuron.* 16:207–218. doi:10.1016/S0896-6273(00)80037-9

Hadley, R.W., and W.J. Lederer. 1991. Ca2+ and voltage inactivate Ca2+ channels in guinea-pig ventricular myocytes through independent mechanisms. *J. Physiol.* 444:257–268.

Hoda, J.C., F. Zaghetto, A. Koschak, and J. Striessnig. 2005. Congenital stationary night blindness type 2 mutations S229P, G369D, L1068P, and W1440X alter channel gating or functional expression of Ca(v)1.4 L-type Ca2+ channels. *J. Neurosci.* 25:252–259. doi:10.1523/JNEUROSCI.3054-04.2005

Hohaus, A., S. Beyl, M. Kudrnac, S. Berjukow, E.N. Timin, R. Marksteiner, M.A. Maw, and S. Hering. 2005. Structural determinants of L-type channel activation in segment IIS6 revealed by a retinal disorder. *J. Biol. Chem.* 280:38471–38477. doi:10.1074/jbc.M507013200

Hoshi, T., W.N. Zagotta, and R.W. Aldrich. 1990. Biophysical and molecular mechanisms of *Shaker* potassium channel inactivation. *Science.* 250:533–538. doi:10.1126/science.2122519

Hoshi, T., W.N. Zagotta, and R.W. Aldrich. 1991. Two types of inactivation in Shaker K+ channels: effects of alterations in the carboxy-terminal region. *Neuron.* 7:547–556. doi:10.1016/0896-6273(91)90367-9

Huber, I., E. Wappl, A. Herzog, J. Mitterdorfer, H. Glossmann, T. Langer, and J. Striessnig. 2000. Conserved Ca2+-antagonist-binding properties and putative folding structure of a recombinant high-affinity dihydropyridine-binding domain. *Biochem. J.* 347:829–836. doi:10.1042/0264-6021:3470829

Imredy, J.P., and D.T. Yue. 1994. Mechanism of $Ca^{(2+)}$-sensitive inactivation of L-type Ca^{2+} channels. *Neuron.* 12:1301–1318. doi:10.1016/0896-6273(94)90446-4

Jacobs, A., B.P. Knight, K.T. McDonald, and M.C. Burke. 2006. Verapamil decreases ventricular tachyarrhythmias in a patient with Timothy syndrome (LQT8). *Heart Rhythm.* 3:967–970. doi:10.1016/j.hrthm.2006.04.024

Jiang, Y., A. Lee, J. Chen, V. Ruta, M. Cadene, B.T. Chait, and R. MacKinnon. 2003. X-ray structure of a voltage-dependent K+ channel. *Nature.* 423:33–41. doi:10.1038/nature01580

Jones, L.P., S.K. Wei, and D.T. Yue. 1998. Mechanism of auxiliary subunit modulation of neuronal α_{1E} calcium channels. *J. Gen. Physiol.* 112:125–143. doi:10.1085/jgp.112.2.125

Jones, L.P., C.D. DeMaria, and D.T. Yue. 1999. N-type calcium channel inactivation probed by gating-current analysis. *Biophys. J.* 76:2530–2552. doi:10.1016/S0006-3495(99)77407-2

Kim, J., S. Ghosh, D.A. Nunziato, and G.S. Pitt. 2004. Identification of the components controlling inactivation of voltage-gated Ca2+ channels. *Neuron.* 41:745–754. doi:10.1016/S0896-6273(04)00081-9

Kraus, R.L., M.J. Sinnegger, H. Glossmann, S. Hering, and J. Striessnig. 1998. Familial hemiplegic migraine mutations change alpha1A Ca2+ channel kinetics. *J. Biol. Chem.* 273:5586–5590. doi:10.1074/jbc.273.10.5586

Kraus, R.L., M.J. Sinnegger, A. Koschak, H. Glossmann, S. Stenirri, P. Carrera, and J. Striessnig. 2000. Three new familial hemiplegic migraine mutants affect P/Q-type Ca(2+) channel kinetics. *J. Biol. Chem.* 275:9239–9243. doi:10.1074/jbc.275.13.9239

Lee, A., S.T. Wong, D. Gallagher, B. Li, D.R. Storm, T. Scheuer, and W.A. Catterall. 1999. Ca2+/calmodulin binds to and modulates P/Q-type calcium channels. *Nature.* 399:155–159. doi:10.1038/20194

Lee, A., H. Zhou, T. Scheuer, and W.A. Catterall. 2003. Molecular determinants of Ca(2+)/calmodulin-dependent regulation of Ca(v)2.1 channels. *Proc. Natl. Acad. Sci. USA.* 100:16059–16064. doi:10.1073/pnas.2237000100

Li, R.A., I.L. Ennis, R.J. French, S.C. Dudley Jr., G.F. Tomaselli, and E. Marbán. 2001. Clockwise domain arrangement of the sodium channel revealed by (mu)-conotoxin (GIIIA) docking orientation. *J. Biol. Chem.* 276:11072–11077. doi:10.1074/jbc.M010862200

Lipkind, G.M., and H.A. Fozzard. 2003. Molecular modeling of interactions of dihydropyridines and phenylalkylamines with the inner pore of the L-type Ca2+ channel. *Mol. Pharmacol.* 63:499–511. doi:10.1124/mol.63.3.499

Liu, Y., M. Holmgren, M.E. Jurman, and G. Yellen. 1997. Gated access to the pore of a voltage-dependent K+ channel. *Neuron.* 19:175–184. doi:10.1016/S0896-6273(00)80357-8

Loots, E., and E.Y. Isacoff. 2000. Molecular coupling of S4 to a K^+ channel's slow inactivation gate. *J. Gen. Physiol.* 116:623–636. doi:10.1085/jgp.116.5.623

López-Barneo, J., T. Hoshi, S.H. Heinemann, and R.W. Aldrich. 1993. Effects of external cations and mutations in the pore region

on C-type inactivation of Shaker potassium channels. *Receptors Channels.* 1:61–71.

Mori, M.X., M.G. Erickson, and D.T. Yue. 2004. Functional stoichiometry and local enrichment of calmodulin interacting with Ca2+ channels. *Science.* 304:432–435. doi:10.1126/science.1093490

Opatowsky, Y., C.C. Chen, K.P. Campbell, and J.A. Hirsch. 2004. Structural analysis of the voltage-dependent calcium channel beta subunit functional core and its complex with the alpha 1 interaction domain. *Neuron.* 42:387–399. doi:10.1016/S0896-6273(04)00250-8

Perez-Reyes, E., A. Castellano, H.S. Kim, P. Bertrand, E. Baggstrom, A.E. Lacerda, X.Y. Wei, and L. Birnbaumer. 1992. Cloning and expression of a cardiac/brain beta subunit of the L-type calcium channel. *J. Biol. Chem.* 267:1792–1797.

Peterson, B.Z., C.D. DeMaria, J.P. Adelman, and D.T. Yue. 1999. Calmodulin is the Ca^{2+} sensor for Ca2+-dependent inactivation of L-type calcium channels. *Neuron.* 22:549–558. doi:10.1016/S0896-6273(00)80709-6

Pietrobon, D. 2007. Familial hemiplegic migraine. *Neurotherapeutics.* 4:274–284. doi:10.1016/j.nurt.2007.01.008

Pitt, G.S., R.D. Zühlke, A. Hudmon, H. Schulman, H. Reuter, and R.W. Tsien. 2001. Molecular basis of calmodulin tethering and Ca2+-dependent inactivation of L-type Ca2+ channels. *J. Biol. Chem.* 276:30794–30802. doi:10.1074/jbc.M104959200

Pragnell, M., J. Sakamoto, S.D. Jay, and K.P. Campbell. 1991. Cloning and tissue-specific expression of the brain calcium channel beta-subunit. *FEBS Lett.* 291:253–258. doi:10.1016/0014-5793(91)81296-K

Raybaud, A., Y. Dodier, P. Bissonnette, M. Simoes, D.G. Bichet, R. Sauvé, and L. Parent. 2006. The role of the GX9GX3G motif in the gating of high voltage-activated Ca2+ channels. *J. Biol. Chem.* 281:39424–39436. doi:10.1074/jbc.M607405200

Raybaud, A., E.E. Baspinar, F. Dionne, Y. Dodier, R. Sauvé, and L. Parent. 2007. The role of distal S6 hydrophobic residues in the voltage-dependent gating of CaV2.3 channels. *J. Biol. Chem.* 282:27944–27952. doi:10.1074/jbc.M703895200

Shen, Y., D. Yu, H. Hiel, P. Liao, D.T. Yue, P.A. Fuchs, and T.W. Soong. 2006. Alternative splicing of the Ca(v)1.3 channel IQ domain, a molecular switch for Ca2+-dependent inactivation within auditory hair cells. *J. Neurosci.* 26:10690–10699. doi:10.1523/JNEUROSCI.2093-06.2006

Shirokov, R., R. Levis, N. Shirokova, and E. Ríos. 1993. Ca^{2+}-dependent inactivation of cardiac L-type Ca^{2+} channels does not affect their voltage sensor. *J. Gen. Physiol.* 102:1005–1030. doi:10.1085/jgp.102.6.1005

Sicouri, S., K.W. Timothy, A.C. Zygmunt, A. Glass, R.J. Goodrow, L. Belardinelli, and C. Antzelevitch. 2007. Cellular basis for the electrocardiographic and arrhythmic manifestations of Timothy syndrome: effects of ranolazine. *Heart Rhythm.* 4:638–647. doi:10.1016/j.hrthm.2006.12.046

Splawski, I., K.W. Timothy, L.M. Sharpe, N. Decher, P. Kumar, R. Bloise, C. Napolitano, P.J. Schwartz, R.M. Joseph, K. Condouris, et al. 2004. Ca(V)1.2 calcium channel dysfunction causes a multisystem disorder including arrhythmia and autism. *Cell.* 119:19–31. doi:10.1016/j.cell.2004.09.011

Splawski, I., K.W. Timothy, N. Decher, P. Kumar, F.B. Sachse, A.H. Beggs, M.C. Sanguinetti, and M.T. Keating. 2005. Severe arrhythmia disorder caused by cardiac L-type calcium channel mutations. *Proc. Natl. Acad. Sci. USA.* 102:8089–8096. doi:10.1073/pnas.0502506102

Stotz, S.C., and G.W. Zamponi. 2001. Identification of inactivation determinants in the domain IIS6 region of high voltage-activated calcium channels. *J. Biol. Chem.* 276:33001–33010. doi:10.1074/jbc.M104387200

Stotz, S.C., J. Hamid, R.L. Spaetgens, S.E. Jarvis, and G.W. Zamponi. 2000. Fast inactivation of voltage-dependent calcium channels. A hinged-lid mechanism? *J. Biol. Chem.* 275:24575–24582. doi:10.1074/jbc.M000399200

Stotz, S.C., S.E. Jarvis, and G.W. Zamponi. 2004. Functional roles of cytoplasmic loops and pore lining transmembrane helices in the voltage-dependent inactivation of HVA calcium channels. *J. Physiol.* 554:263–273. doi:10.1113/jphysiol.2003.047068

Swartz, K.J. 2008. Sensing voltage across lipid membranes. *Nature.* 456:891–897. doi:10.1038/nature07620

Tadross, M.R., and D.T. Yue. 2010. Systematic mapping of the state dependence of voltage- and Ca^{2+}-dependent inactivation using simple open-channel measurements. *J. Gen. Physiol.* 135:217–227.

Tadross, M.R., I.E. Dick, and D.T. Yue. 2008. Mechanism of local and global Ca2+ sensing by calmodulin in complex with a Ca2+ channel. *Cell.* 133:1228–1240. doi:10.1016/j.cell.2008.05.025

Tomlinson, W.J., A. Stea, E. Bourinet, P. Charnet, J. Nargeot, and T.P. Snutch. 1993. Functional properties of a neuronal class C L-type calcium channel. *Neuropharmacology.* 32:1117–1126. doi:10.1016/0028-3908(93)90006-O

Van Petegem, F., K.A. Clark, F.C. Chatelain, and D.L. Minor Jr. 2004. Structure of a complex between a voltage-gated calcium channel beta-subunit and an alpha-subunit domain. *Nature.* 429:671–675. doi:10.1038/nature02588

Vitko, I., A. Shcheglovitov, J.P. Baumgart, I.I. Arias-Olguín, J. Murbartián, J.M. Arias, and E. Perez-Reyes. 2008. Orientation of the calcium channel beta relative to the alpha(1)2.2 subunit is critical for its regulation of channel activity. *PLoS One.* 3:e3560. doi:10.1371/journal.pone.0003560

West, J.W., D.E. Patton, T. Scheuer, Y. Wang, A.L. Goldin, and W.A. Catterall. 1992. A cluster of hydrophobic amino acid residues required for fast Na(+)-channel inactivation. *Proc. Natl. Acad. Sci. USA.* 89:10910–10914. doi:10.1073/pnas.89.22.10910

Xie, C., X.G. Zhen, and J. Yang. 2005. Localization of the activation gate of a voltage-gated Ca^{2+} channel. *J. Gen. Physiol.* 126:205–212. doi:10.1085/jgp.200509293

Xu, W., and D. Lipscombe. 2001. Neuronal Ca(V)1.3alpha(1) L-type channels activate at relatively hyperpolarized membrane potentials and are incompletely inhibited by dihydropyridines. *J. Neurosci.* 21:5944–5951.

Yang, P.S., B.A. Alseikhan, H. Hiel, L. Grant, M.X. Mori, W. Yang, P.A. Fuchs, and D.T. Yue. 2006. Switching of Ca2+-dependent inactivation of Ca(v)1.3 channels by calcium binding proteins of auditory hair cells. *J. Neurosci.* 26:10677–10689. doi:10.1523/JNEUROSCI.3236-06.2006

Yellen, G., D. Sodickson, T.Y. Chen, and M.E. Jurman. 1994. An engineered cysteine in the external mouth of a K+ channel allows inactivation to be modulated by metal binding. *Biophys. J.* 66:1068–1075. doi:10.1016/S0006-3495(94)80888-4

Yifrach, O., and R. MacKinnon. 2002. Energetics of pore opening in a voltage-gated K(+) channel. *Cell.* 111:231–239. doi:10.1016/S0092-8674(02)01013-9

Zagotta, W.N., T. Hoshi, J. Dittman, and R.W. Aldrich. 1994. Shaker potassium channel gating. II: transitions in the activation pathway. *J. Gen. Physiol.* 103:279–319. doi:10.1085/jgp.103.2.279

Zhang, J.F., P.T. Ellinor, R.W. Aldrich, and R.W. Tsien. 1994. Molecular determinants of voltage-dependent inactivation in calcium channels. *Nature.* 372:97–100. doi:10.1038/372097a0

Zhorov, B.S., E.V. Folkman, and V.S. Ananthanarayanan. 2001. Homology model of dihydropyridine receptor: implications for L-type Ca(2+) channel modulation by agonists and antagonists. *Arch. Biochem. Biophys.* 393:22–41. doi:10.1006/abbi.2001.2484

Zong, S., J. Zhou, and T. Tanabe. 1994. Molecular determinants of calcium-dependent inactivation in cardiac L-type calcium channels. *Biochem. Biophys. Res. Commun.* 201:1117–1123. doi:10.1006/bbrc.1994.1821

Zühlke, R.D., G.S. Pitt, K. Deisseroth, R.W. Tsien, and H. Reuter. 1999. Calmodulin supports both inactivation and facilitation of L-type calcium channels. *Nature.* 399:159–162. doi:10.1038/20200l